



**HAL**  
open science

## Controlling chaotic oscillations in a symmetric two-mass model of the vocal folds

Oriol Guasch, Annemie van Hirtum, Inés Fernández, Marc Arnela

► **To cite this version:**

Oriol Guasch, Annemie van Hirtum, Inés Fernández, Marc Arnela. Controlling chaotic oscillations in a symmetric two-mass model of the vocal folds. *Chaos, Solitons & Fractals*, 2022, 10.1016/j.chaos.2022.112188 . hal-03666299

**HAL Id: hal-03666299**

**<https://hal.science/hal-03666299>**

Submitted on 12 May 2022

**HAL** is a multi-disciplinary open access archive for the deposit and dissemination of scientific research documents, whether they are published or not. The documents may come from teaching and research institutions in France or abroad, or from public or private research centers.

L'archive ouverte pluridisciplinaire **HAL**, est destinée au dépôt et à la diffusion de documents scientifiques de niveau recherche, publiés ou non, émanant des établissements d'enseignement et de recherche français ou étrangers, des laboratoires publics ou privés.

# Controlling chaotic oscillations in a symmetric two-mass model of the vocal folds

Oriol Guasch<sup>a,\*</sup>, Annemie Van Hirtum<sup>b</sup>, Inés A. Fernández<sup>c</sup>, Marc Arnela<sup>a</sup>

<sup>a</sup>*GTM - Grup de Recerca en Tecnologies Mèdia, La Salle, Universitat Ramon Llull  
C/ Quatre Camins 30, 08022 Barcelona, Catalonia, Spain*

<sup>b</sup>*Univ. Grenoble Alpes, CNRS, Grenoble INP, LEGI, 38000 Grenoble, France*

<sup>c</sup>*Dep. of Materials Science and Physical Chemistry, University of Barcelona, Catalonia, Spain*

---

## Abstract

Human phonation is a highly non-linear process in which subglottal flow emanating from the lungs induces self-oscillations of the vocal folds. In normal conditions, this results in the generation of a regularly pulsating volume velocity that becomes the source of acoustic waves, which once modulated by the vocal tract, get emitted outwards as voice. However, vocal folds oscillations can become chaotic under many circumstances. For instance, even in the case of healthy symmetric vocal folds, an excess value of the subglottal pressure can trigger chaotic motion. In this paper, we derive a chaos control strategy for a two-mass model of the vocal cords to revert this situation and render the motion regular again. The approach relies on slightly altering the system energy to move it to a stable state. Given that no external control forces can be applied to the vocal cords, it is proposed to add a third mass to the original two-mass model, which is assumed to be made of an ideal smart material. The mass of the smart material is presumed negligible in comparison to the two masses of the vocal folds model, but its damping and stiffness can be tuned to evolve with time. For a fixed subglottal pressure for which the motion is chaotic, it is shown how periodicity can be recovered using adequate damping laws, by either attaching the smart material onto the larger vocal fold mass or onto the smaller one. For the latter, control turns to be more difficult and the damping of the smart material has to quickly vary with time. On the other hand, given that the subglottal pressure would rarely be constant in a real situation, we also introduce a damping law to avoid chaotic motion as the subglottal pressure augments or diminishes. Finally, it is shown that control can not only be achieved by acting on the damping of the smart material but also on its stiffness. A stiffness law to prevent chaotic oscillations and get a healthy pulsating volume velocity is therefore implemented. A brief discussion on the mid-long term potential of the presented solution for practical cases is included.

*Keywords:* Vocal fold pacemaker, Vocal fold dynamics, Chaotic self-oscillations, Chaos control, Smart materials, Two-mass models

---

## 1. Introduction

The essentials of the myoelastic aerodynamic theory of human phonation are nowadays well understood [1, 2]. In a nutshell, the air emanating from the lungs reaches the larynx and exerts a pressure on the vocal folds which open once surpassed a certain threshold value. This opening causes the pressure to suddenly drop and as a consequence the vocal folds close again until the subglottal pressure becomes strong enough to force a new aperture. In this way, self-oscillations of the vocal folds are established. The regular opening/closing of the vocal cords results in a glottal volume velocity that acts as a source term for the

---

\*Corresponding Author: oriol.guasch@salle.url.edu

39 waves. The latter propagate and become modulated inside the vocal tract and get finally emitted outside  
40 the mouth, as voice.

41 The process of phonation is highly non-linear due to the complex combination of non-linear biomechanics  
42 involving impacts and aerodynamics, and can often lead to chaotic oscillations of the vocal folds, which may  
43 induce abnormal and unpleasant voice. This is often the case in voice pathologies like unilateral paralyses  
44 or in lesions involving nodules, polyps or cysts. To better understand the physics behind those phenomena,  
45 several low-dimensional models of the vocal folds were developed during the past half century, consisting  
46 of mass-spring-damper systems driven by glottal flow excitation. The investigation on the so-called mass  
47 models began in the earlier seventies, being probably the two-mass model of Ishizaka and Flanagan the  
48 most celebrated one [3]. However, it was not until the nineties that non-linear dynamics methods were  
49 used to understand the bifurcation processes that led from regular vocal fold motion to chaotic one (see  
50 e.g., [4–6]). Investigations on lumped mass models of increasing complexity [7–10] continued through the  
51 next decades and low dimensional models for the vocal fold self-oscillations [11–13] and glottal flows [14, 15]  
52 still constitute a very active area of experimental and theoretical research. **In fact, it would be interesting  
53 to check whether advances and new proposals in the classification of attractors and bifurcation theory [16],  
54 like the identification of hidden attractors [17–19] and/or hyperchaos [20–22] could be of relevance for some  
55 of these lumped models of the vocal folds and if they could have physical implications in terms of voice  
56 production.**

57 Despite all efforts made to understand the physical mechanisms of voice disorders, the possibility of  
58 establishing control strategies that could revert chaotic vocal fold vibrations to regular ones have not been  
59 explored yet. **The main novelty of this paper is to examine if that could be feasible or not. To the best of our  
60 knowledge this has not been attempted before. Using low dimensional mass models, we aim at a theoretical  
61 design of a vocal fold pacemaker that could improve voice quality.** It is to be noted that laryngeal pacemakers  
62 have been amongst us for decades [23–25] and recent progress have been achieved on them [26–28]. However,  
63 such pacemakers are not intended at all to deal with voice generation problems but are designed to solve  
64 critical medical problems related to abduction and inspiration.

65 In this paper we will make use of the two-mass model in [5] and propose a control approach for chaotic  
66 vocal fold oscillations. To facilitate the analysis we will deal with the easiest case in which the two-mass  
67 model is totally symmetric, i.e. there are no geometrical or physical differences between the left and right  
68 vocal cords. It was shown in [29] that even in this simple situation chaotic motion could arise for high  
69 enough subglottal pressure values. This results in irregular glottal volume velocity and, therefore, in poor  
70 voice quality. There exist several feedback chaos control schemes that are useful for non-linear mechanical  
71 systems involving impacts, like the ones we encounter in the modelling of the vocal folds. The popular  
72 Ott-Grebogi-Yorke (OGY) strategy [30] essentially locates an unstable periodic orbit embedded in a chaotic  
73 attractor and then stabilizes the orbit by inducing small perturbations on a control parameter. The OGY  
74 method has been successfully applied to a large variety of problems and it performs well in those with impacts,  
75 see e.g. [31]. On the other hand, since the proposal of delayed feedback control strategies in [32, 33] a vast  
76 amount of feedback control algorithms have been successfully developed (see e.g., the reviews in [34–36]),  
77 which have also turned to be very efficient in stabilizing a large variety of mechanical problems that include  
78 contact [37–40]. More recently, another feedback strategy was suggested which does not require knowing  
79 the system equations and basically relies on its output time series [41, 42]. The basic idea in [41, 42] is  
80 to slightly alter the time averaged oscillation energy (kinetic plus potential) of the system to move it to a  
81 value where it becomes stable. Such approach has proved valid for classical non-linear oscillators (e.g., Van  
82 der Pol and Duffing oscillators), for networks of oscillators, and for colliding elements as well [43]. Given  
83 that our two-mass model driven by the glottal flow involves more than one mass and also deals with contact  
84 between vocal folds, we have relied on the strategy in [41, 42] to help transitioning the chaotic motion of  
85 the vocal folds to periodic one, and get an appropriate glottal volume velocity. It is to be remarked that  
86 the volume velocity will be our variable of primary interest throughout the paper.

87 **The main novel contributions of this work are as follows.** First, let us note that most chaos controlling  
88 approaches, like that in [41, 42], depend on applying an external control force to stabilize the system. Given  
89 that this would not be possible in the case of the vocal folds, our proposal is to substitute that force by the  
90 inclusion of a third mass, made of a smart material, in the original two-mass model of the vocal folds. The

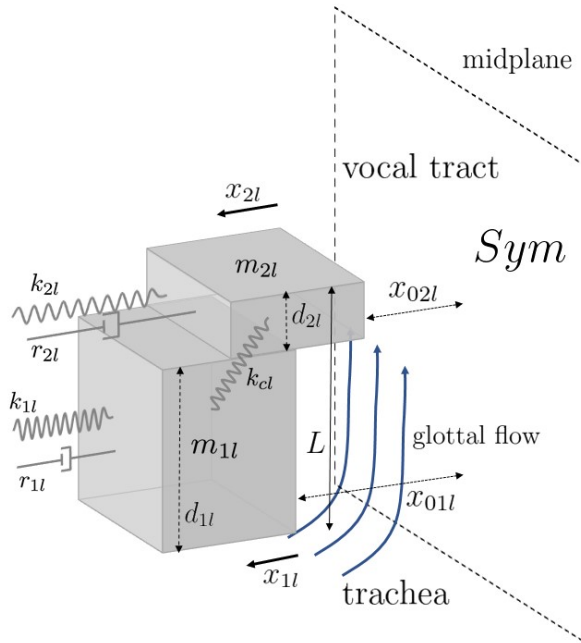


Figure 1: Schematic representation of the two-mass model of the vocal folds described by Eq. (4). As we are considering the symmetric case, only the left vocal cords and its associated variables and parameters are represented.

91 smart material is assumed to be ideal in the sense of its mass being negligible in comparison to the lower  
 92 large mass and upper small mass of the vocal folds model, and also in the sense of having the property  
 93 that its damping and stiffness can be tuned to evolve with time without restrictions. In some way, the  
 94 suggested strategy corresponds to swapping the external control force from the right hand side of the system  
 95 of equations to the left hand side, and integrate it as an internal force with variable parameters. After  
 96 establishing the new model, we propose different laws for reverting the vocal cords motion from chaotic  
 97 to periodic. For a fixed subglottal pressure value, if one attaches the smart material to the large mass of  
 98 the vocal folds it suffices to increase the overall damping value to transition to a stable state. However,  
 99 achieving control by gluing the smart material to the small mass is by far more subtle and the time evolving  
 100 law in [41, 42] becomes necessary to get a robust solution, in which the vocal folds still collide closing the  
 101 glottis. On the other hand, given that in practice the subglottal pressure that drives the vocal cord self-  
 102 oscillations will not be constant, we introduce a new feedback mechanism to guarantee a periodic volume  
 103 velocity in such situation. Finally, we show that chaos control can not only be achieved by modifying the  
 104 damping of the smart material but also by changing its stiffness. An appropriate law is introduced to do so.

105 The paper is organized as follows. In section 2, we present the ODE system corresponding to the  
 106 symmetric two-mass model in [5, 29]. Section 3 contains a brief review of the performance of that model  
 107 when varying the subglottal pressure and the contact stiffness between masses. Special emphasis is placed  
 108 on the consequences for the glottal volume velocity when transitioning to chaotic motion. In section 4, we  
 109 start reviewing the control strategy in [41, 42] and then propose the idea of applying it to our problem by  
 110 including a third smart material mass into the system. The section continues by exploring several damping  
 111 laws to either control the large mass or the small mass of the system and analyses the impact that this  
 112 has on the volume velocity. Then, the case of non-constant subglottal pressure is addressed and a chaos  
 113 control approach is derived for it. Finally, it is shown that stabilization can also be achieved by modifying  
 114 the stiffness of the smart material. A short discussion follows considering the mid-long term potential of  
 115 the proposed theoretical solution based on currently existing smart materials and their properties [44]. The  
 116 conclusions close the paper in section 5.

117 **2. Non-linear ODE system for the symmetric vocal fold two-mass model**

118 Through years, several models have been proposed to simulate the underlying physics of phonation and  
 119 in particular the onset of self-oscillations of the vocal folds. The latter are located in the larynx, which  
 120 connects the trachea and the vocal tract, and can be mechanically represented as a distributed system of  
 121 masses, springs and dampers. The glottis is the opening between vocal folds. The easiest models that are  
 122 able to reproduce the essential physiological and mechanical properties of phonation, namely the interaction  
 123 between the vocal fold geometry and the glottal airflow obeying Bernoulli's equation are the two-mass  
 124 models [3]. In such models, a vocal cord is separated in depth (thickness) into an upper and lower part,  
 125 each one consisting of an oscillator characterized by mass, stiffness and damping values (see Fig. 1). If one  
 126 considers the case of symmetric vocal folds, it suffices to study the dynamics of either the right or left ones.  
 127 The latter have been chosen in this work. The phase lag between the lower and upper masses  $m_{1l}$  and  $m_{2l}$   
 128 in Fig. 1 is essential for the generation of self-sustained oscillations, which can not be reproduced by single  
 129 mass models.

Assuming that the cubic nonlinearity of the oscillators in the Ishizaka and Flanagan two-mass model is small, that the interaction of the vocal folds and glottal flow dynamics are independent of subglottal and supraglottal resonances in the trachea and vocal tract, and that the approximation of Bernoulli's flow applies, the equations of motion for  $m_{1l}$  and  $m_{2l}$  can be derived from Newton's second law (see e.g., [5, 29] for more details),

$$m_{1l}\ddot{x}_{1l} + r_{1l}\dot{x}_{1l} + k_{1l}x_{1l} + k_{cl}(x_{1l} - x_{2l}) + \Theta(-a_1)c_{1l}\frac{a_1}{2L} = P_1 L d_{1l}, \quad (1a)$$

$$m_{2l}\ddot{x}_{2l} + r_{2l}\dot{x}_{2l} + k_{2l}x_{2l} + k_{cl}(x_{2l} - x_{1l}) + \Theta(-a_2)c_{2l}\frac{a_2}{2L} = 0, \quad (1b)$$

where,  $r_{il}$  ( $i = 1, 2$ ) stand for the damping constants,  $k_{il}$  ( $i = 1, 2$ ) for the stiffness ones and  $k_{cl}$  is the coupling stiffness between the upper and lower masses (see Fig. 1). The dampers  $r_{il}$  account for the mass stickiness when the moist surfaces of the left and right vocal folds do have contact [3]. The springs with stiffness  $k_{il}$  are a representation of the tension of the vocal folds, which is controlled by the contraction of the anterior cricothyroid muscle, among others [2, 3]. In what concerns the coupling stiffness,  $k_{cl}$ , it characterizes the flexural stiffness in the lateral direction of the vocal cords. Likewise, the fifth term on the left hand side (l.h.s) of Eqs. (1a) and (1b) is the non-linear collision force between the right and left vocal folds.  $a_i = a_{0i} + 2Lx_{il}$  ( $i=1,2$ ) are the lower and upper glottal areas with  $L$  being the length of the glottis and  $a_{0i} = 2Lx_{0il}$  ( $i=1,2$ ) the lower and upper glottal rest areas ( $x_{0il}$  stands for the distance of  $m_{il}$  to the midline in the rest position). The collision function  $\Theta$  is approximated by  $\Theta(z) = \tanh(50z/z_0)$  for  $z > 0$  and becomes zero if  $z \leq 0$ .  $z_0$  is taken as  $a_{01}$  in the computations.  $c_{il}$  ( $i = 1, 2$ ) are additional spring constants during collision. As regards the force term in the right hand side (r.h.s) of Eq. (1a),  $d_{1l}$  is the thickness of  $m_{1l}$  and  $P_1$  is the glottal pressure acting on it. Bernoulli's equation allows one to derive the following expression for  $P_1$ ,

$$P_1 = P_s \left[ 1 - \Theta(a_{\min}) \left( \frac{a_{\min}}{a_1} \right)^2 \right] \Theta(a_1), \quad (2)$$

130 with  $P_s$  being the subglottal pressure and  $a_{\min} = a_1$  if  $x_{1l} < x_{2l}$  while  $a_{\min} = a_2$  if  $x_{2l} \leq x_{1l}$ .

An important parameter for voice generation is the volume flow velocity,  $U$ . This acts as a source term which excites acoustic waves in the vocal tract that become radiated as voice outside the mouth.  $U$  is typically prescribed as a boundary condition at the glottis in numerical voice production studies (see e.g., [45–48]). The volume flow velocity can be computed as,

$$U = \left( \frac{2P_s}{\rho} \right)^{1/2} a_{\min} \Theta(a_{\min}). \quad (3)$$

Eqs. (1a) and (1b) can be converted into a first-order non-linear ODE system of the type  $\dot{\mathbf{y}} = \mathbf{A}(\mathbf{y})\mathbf{y} + \mathbf{f}(\mathbf{y})$  by introducing the mass velocities  $v_{1l} = \dot{x}_{1l}$  and  $v_{2l} = \dot{x}_{2l}$  as independent variables. This yields,

$$\begin{aligned} \dot{\mathbf{y}} \equiv \begin{pmatrix} \dot{\mathbf{v}} \\ \dot{\mathbf{x}} \end{pmatrix} &= \begin{pmatrix} -\mathbf{M}^{-1}\mathbf{C} & -\mathbf{M}^{-1}(\mathbf{K} + \Theta(\mathbf{x})) \\ \mathbf{I} & \mathbf{0} \end{pmatrix} \begin{pmatrix} \mathbf{v} \\ \mathbf{x} \end{pmatrix} + \begin{pmatrix} \mathbf{M}^{-1}\mathbf{f}_v(\mathbf{x}) \\ \mathbf{0} \end{pmatrix} \\ &\equiv \mathbf{A}(\mathbf{y})\mathbf{y} + \mathbf{f}(\mathbf{y}) \equiv \mathbf{g}(\mathbf{y}), \end{aligned} \quad (4)$$

where  $\mathbf{v} = (v_{1l}, v_{2l})^\top$  is the mass velocity vector and  $\mathbf{x} = (x_{1l}, x_{2l})^\top$  the displacement one, so that  $\mathbf{y} = (\mathbf{v}, \mathbf{x})^\top$ , as identified in Eq. (4). The force vector component is given by  $\mathbf{f}_v = (P_1 L d_{1l}, 0)^\top$ . It is also common to express Eq. (4) as  $\dot{\mathbf{y}} = \mathbf{g}(\mathbf{y})$ , with  $\mathbf{g}(\mathbf{y}) = \mathbf{A}(\mathbf{y})\mathbf{y} + \mathbf{f}(\mathbf{y})$ , as shown in the last equality of Eq. (4). The block matrices in  $\mathbf{A}$  correspond to the identity  $\mathbf{I}$ , and to the mass,  $\mathbf{M}$ , damping,  $\mathbf{C}$ , stiffness,  $\mathbf{K}$  and collision,  $\Theta$ , matrices given by,

$$\begin{aligned} \mathbf{M} &= \text{diag}(m_{1l}, m_{2l}), & \mathbf{C} &= \text{diag}(r_{1l}, r_{2l}), \\ \mathbf{K} &= \begin{pmatrix} k_{1l} + k_{cl} & -k_{cl} \\ -k_{cl} & k_{2l} + k_{cl} \end{pmatrix} & \Theta &= \text{diag} \left( \Theta(-a_1)c_{1l} \left[ \frac{a_{01}}{2Lx_{1l}} + 1 \right], \Theta(-a_2)c_{2l} \left[ \frac{a_{02}}{2Lx_{2l}} + 1 \right] \right). \end{aligned} \quad (5)$$

131 Note that the non-linearity enters the ODE system through  $\Theta(\mathbf{x})$  and  $\mathbf{f}_v(\mathbf{x})$ . The dynamics of Eq. (4)  
 132 has been analysed at extent in [5, 29], showing that for slightly higher values of the coupling constant  $k_{cl}$   
 133 than usual, and for large subglottal pressure values,  $P_s$ , the motion of the two vocal fold masses can become  
 134 aperiodic, or even chaotic. We will briefly review some of these aspects in the following section. It is to be  
 135 noted that such abnormal behaviour of the vocal folds can have a profound impact on the glottal volume  
 136 flow velocity  $U$ , and therefore, in the quality of the generated voice.

### 137 3. Chaotic motion of the vocal folds at high subglottal pressure and effects on the glottal 138 volume flow velocity

139 For subsequent simulations, the physical and geometrical parameters in Table 1 have been employed.  
 140 Throughout this text, the dimensions of the various variables will not be written (though they will be explic-  
 141 itly indicated in figures). They correspond to appropriate combinations of taking the following dimensions  
 142 for length  $[L] = \text{cm}$ , time  $[T] = \text{ms}$  and mass  $[M] = \text{g}$ . It is to be noted that the standard value for the  
 143 coupling stiffness of  $k_{cl} = 0.025$  has been increased to  $k_{cl} = 0.09$  in the simulations following [29]. As said,  
 144 the system in Eq. (4) was studied in detail in the past. Its dynamic behaviour dependence on the values  
 145 of various model parameters was investigated and standard methods of non-linear analysis were applied  
 146 to it. In [5], the existence and stability of fixed points was addressed through linearisation, while in [29]  
 147 a combination of techniques were used to discriminate under which conditions the motion of the masses  
 148 becomes chaotic. The authors found that the system exhibits one positive Lyapunov exponent for large  
 149 enough subglottal pressure values, which proves the existence of chaos (a Kaplan-Yorke dimension of 2.4  
 150 was reported indicating low-dimensional chaos). **Despite being four dimensional, hyperchaos is therefore not  
 151 possible in this particular system because at least two positive Lyapunov exponents are necessary for that  
 152 to occur (see e.g. [20–22]).** Strange attractors at the phase spaces of the two masses were reported in [29], as  
 153 well as broadband noisy spectra and complex Poincaré sections. Bifurcation plots for the mass displacement  
 154 amplitudes in terms of  $k_{cl}$ ,  $P_s$  and further parameters were shown pointing out to a period doubling route  
 155 to chaos.

156 In this section, we will only outline the essentials of the behaviour of the system in Eq. (4) in a nutshell.  
 157 The interested reader is referred to the original works [5, 29] for details. In contrast to the general approach  
 158 in [5, 29], however, special emphasis will be placed herein on the effects that the vocal fold dynamics have  
 159 on the volume velocity  $U$ . All simulations in this work have been carried out implementing a standard  
 160 fourth-order Runge-Kutta numerical method.

161 One can basically distinguish three different regimes for the vocal folds motion when we fix all system  
 162 parameters but progressively increase the subglottal pressure  $P_s$ . These are captured in Fig. 2, where we  
 163 plot different type of results for  $P_s = \{0.0035, 0.021, 0.036\}$ . Each row in the figure corresponds to a value

164 of  $P_s$  that is representative of such regimes. The first column contains trajectories in the phase space for  $m_{1l}$ ,  
 165 the second column shows the time evolution of  $x_{1l}$  and the third one plots the time evolution of  $U$ . **The**  
 166 **results for  $m_{2l}$  are very similar to those of  $m_{1l}$  and add no physical insight into the problem. Consequently**  
 167 **they have not been included for the sake of brevity.** The blue lines in the figure have been obtained from  
 168 the solution of Eq. (4) using the set of initial conditions  $\mathbf{y}_1(0) = (0, 0, 0.1, 0.1)^\top$ , while the red dashed ones  
 169 correspond to the neighbouring initial condition  $\mathbf{y}_2(0) = (0, 0, 0.11, 0.11)^\top$ .

170 If we focus on the first row of the figure we observe that the pressure  $P_s = 0.0035$  is unable to generate  
 171 self-oscillations of the vocal folds. The trajectories in phase space are spirals that decay from the initial  
 172 condition to the fixed point  $(0, 0)$ , i.e. the mass  $m_{1l}$  reaches the zero rest position where it stands still.  
 173 Observe that the two spirals in the figure corresponding to the initial conditions  $\mathbf{y}_1(0)$  and  $\mathbf{y}_2(0)$  remain  
 174 close to each other until they reach the origin. As regards the time evolution of  $x_{1l}$ , it shows a few oscillations  
 175 until the mass stops. Again, the two lines in the figure remain very close one to each other but do not match.  
 176 The glottal volume flow velocity  $U$  in the third subfigure of the first row becomes zero in a few occasions  
 177 because of the impact between vocal folds, and then acquires a small residual constant value because the  
 178 vocal folds do not contact in the rest position.

179 The situation in the second row would be the desirable one for voice generation (taking into account  
 180 the very severe simplifications assumed in the model of Eq. (4)). When the subglottal pressure increases,  
 181 at some point the solution exhibits a Hopf bifurcation and a limit cycle in phase space is formed. It can be  
 182 observed in the first figure of the second row, that the two trajectories arising from  $\mathbf{y}_1(0)$  and  $\mathbf{y}_2(0)$  merge  
 183 at the limit cycle and then oscillate with exactly the same time period (see the plot of  $x_{1l}$  versus time).  
 184 The volume flow velocity is also periodic, as observed in the third figure of the second row. It remains zero  
 185 during the vocal fold impacts, then increases to a maximum and then decreases again until the next impact  
 186 occurs.

187 The conditions in the third row are the undesirable ones. As long as  $P_s$  grows, the system bifurcates  
 188 again and the periodicity of the vocal fold self-oscillations is lost. For  $P_s = 0.041$  the motion has already  
 189 become chaotic, exhibiting a strong sensitivity to the initial conditions. This is apparent in the phase space  
 190 plot, where strange attractors are observed and the trajectories starting from  $\mathbf{y}_1(0)$  and  $\mathbf{y}_2(0)$  quickly depart  
 191 from each other. If we look at the plot of  $x_{1l}$  versus time, we also perceive that, after a few oscillations, the  
 192 evolution of  $x_{1l}$  when starting at  $\mathbf{y}_1(0)$  clearly differs from that starting at  $\mathbf{y}_2(0)$ . The motion is no longer  
 193 periodic at all and exhibits sudden amplitude transitions. The same occurs for the volume flux velocity:  
 194 neither the impacts nor the amplitudes of  $U$  are regular. Such circumstance could result in a severe loss of  
 195 quality of the generated voice.

196 To better recognize the effects of the chaotic mass motion on the glottal volume flow velocity,  $U$ , in the  
 197 first row of Fig. 3 we have taken advantage of Takens's theorem to recover the attractor in the phase space  
 198  $(\dot{U}, U)$  by plotting  $(U(t+\tau), U(t))$ . Here,  $\tau$  is a time lag. There are different options for choosing  $\tau$  (e.g., one  
 199 could take the first local minimum of the mutual information usually applied to determine the correlation  
 200 dimension in time series analysis [49] c.f., [50]). For our purposes, a simpler option suffices. We have taken

| Physical parameters                  | Geometry parameters          |
|--------------------------------------|------------------------------|
| $m_{1l} = 2.5 \text{ g}$             | $d_{1l} = 0.25 \text{ cm}$   |
| $m_{2l} = 0.125 \text{ g}$           | $d_{2l} = 0.05 \text{ cm}$   |
| $r_{1l} = 0.02 \text{ g ms}^{-1}$    | $L = 1.4 \text{ cm}$         |
| $r_{2l} = 0.01 \text{ g ms}^{-1}$    | $a_{01} = 0.05 \text{ cm}^2$ |
| $k_{1l} = 0.08 \text{ g ms}^{-2}$    | $a_{02} = 0.05 \text{ cm}^2$ |
| $k_{2l} = 0.008 \text{ g ms}^{-2}$   |                              |
| $k_{cl} = 0.09 \text{ g ms}^{-2}$    |                              |
| $c_{1l} = 3k_{1l} \text{ g ms}^{-2}$ |                              |
| $c_{2l} = 3k_{2l} \text{ g ms}^{-2}$ |                              |
| $\rho = 0.00113 \text{ g cm}^{-3}$   |                              |

Table 1: Physical and geometrical parameters of the vocal folds (see [5, 29]).

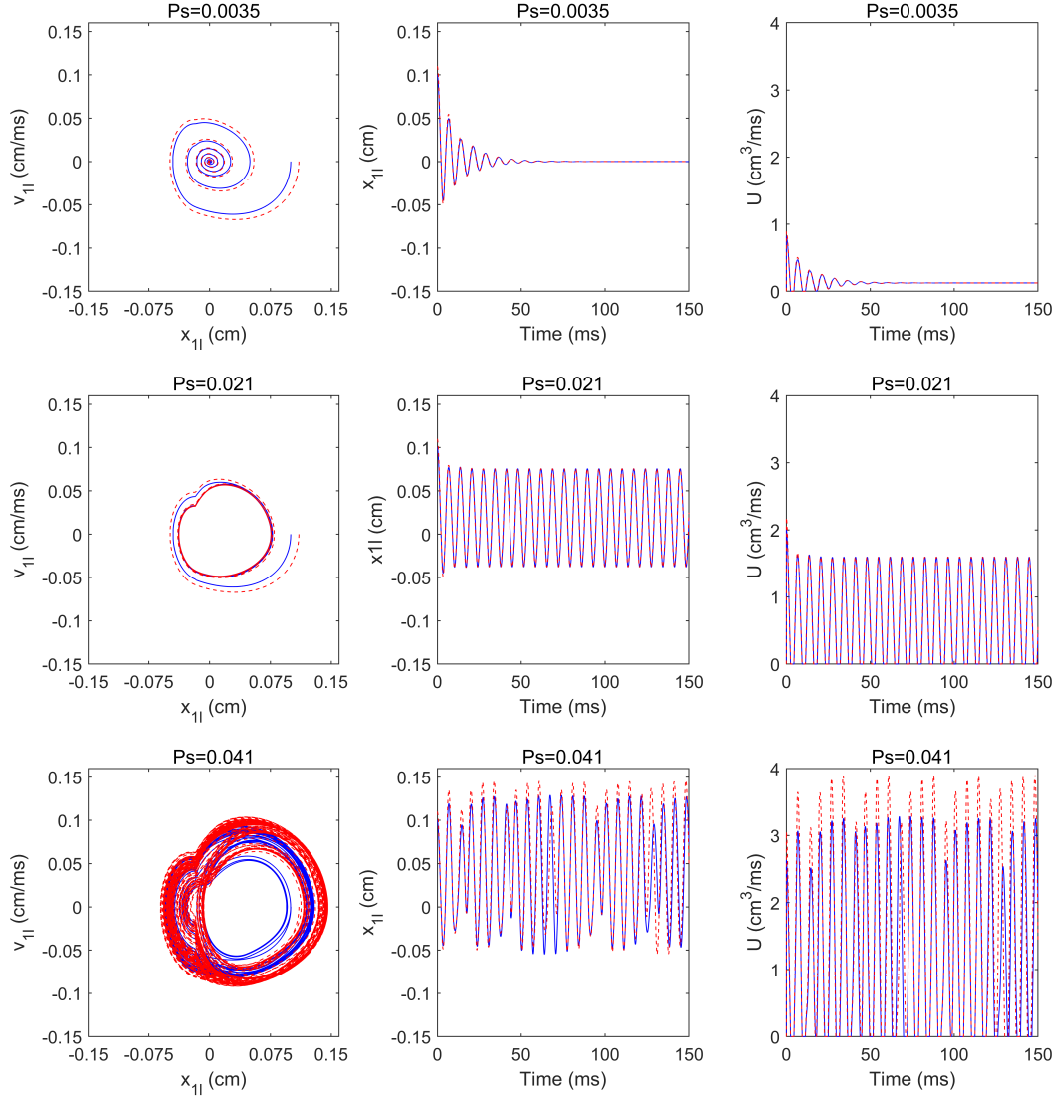


Figure 2: Vocal fold dynamics for different values of the subglottal pressure  $P_s$ . Blue line: set of initial conditions  $\mathbf{y}_1(0)$ . Red dashed line: set of initial conditions  $\mathbf{y}_2(0)$ . Left column: phase space plot of  $v_{1l}$  versus  $x_{1l}$  for mass  $m_{1l}$ . Mid column: time evolution of the position  $x_{1l}$  of  $m_{1l}$ . Right column: time evolution of the glottal volume flow velocity.

201  $\tau = 4T_{P_s=0.021} = 27.56$  with  $T_{P_s=0.021}$  being the period of  $U$  when the pressure is  $P_s = 0.021$  (see Fig. 2,  
202 second row, third column), which results in the blue line of the left-top subfigure in Fig. 3. Note that if we  
203 chose a different time delay, like  $\tau = 20$ , we get an homeomorphic result to the previous one (green line in  
204 the figure). However, when we increase the subglottal pressure to  $P_s = 0.041$ , a strange attractor develops  
205 in the phase space of  $U$ , as illustrated in the right-top plot of Fig. 3. While in the results of Fig. 2 the initial  
206 transients were included to show the dependence on initial conditions, Fig. 3 does not contemplate them.  
207 For completeness, in the bottom row of Fig. 3 we have plotted the value of  $U$  depending on the positions  $x_{1l}$

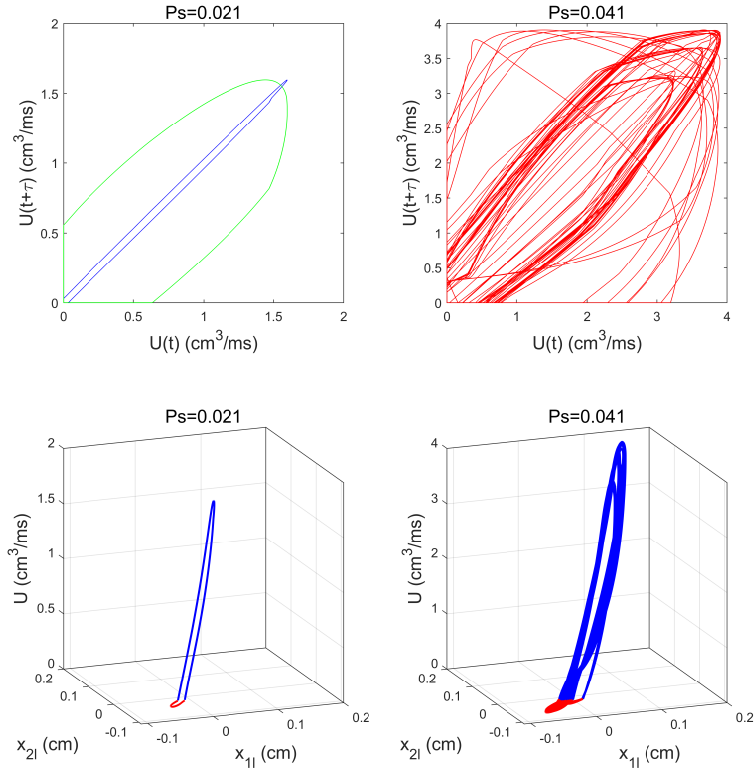


Figure 3: First row: phase space plot for the glottal volume velocity  $U(t + \tau)$  versus  $U(t)$  for  $P_s = 0.021$  and  $P_s = 0.041$ . Second row: volume velocity depending on the position of the two masses  $x_{1l}$  and  $x_{2l}$ , i.e.,  $U(x_{1l}, x_{2l})$ . The red colour indicates zero values for  $U$  which occurs when the left and right masses do contact. Different scales have been used to better appreciate the difference between plots.

208 and  $x_{2l}$  of the two masses, namely  $U(x_{1l}, x_{2l})$ . The red colour indicates the values of  $x_{1l}$  and  $x_{2l}$  for which  
 209  $U$  equals zero, i.e. either the left first or second masses contact the right ones and no volume flow can pass  
 210 through the glottis. The blue colour corresponds to positive values of  $U$ . The comparison between the two  
 211 figures in the bottom row supports the information found from the attractors in the top row. Setting the  
 212 subglottal pressure to  $P_s = 0.041$  entails an abnormal, chaotic, behaviour of the motion of the masses and  
 213 hence of  $U$ . Please note that different scales have been used for the left and right columns of Fig. 3 for  
 214 better inspection, as increasing  $P_s$  from 0.021 to 0.041 implies a significant growth of the amplitude of the  
 215 volume velocity.

216 Finally, and to complete this brief overview on the behaviour of the symmetric two-mass model, in Fig. 4  
 217 we have plotted bifurcation plots of the maximum amplitude displacements of  $m_{1l}$ , namely  $\max |x_{1l}|$ , for two  
 218 different situations. The left subfigure corresponds to fixing the subglottal pressure at  $P_s = 0.041$  and then  
 219 increasing the coupling stiffness constant from  $k_{cl} = 0.025$  to  $k_{cl} = 0.09$ . As illustrated in the figure, for low  
 220 values of  $k_{cl}$  the motion remains periodic but for  $k_{cl}$  close to 0.057 it becomes chaotic. Then, a window of  
 221 aperiodic motion can be observed until the motion becomes chaotic again. In contrast, in the right subfigure  
 222 we have kept  $k_{cl} = 0.09$  fixed and changed the subglottal pressure from  $P_s = 0.0001$  to  $P_s = 0.08$ . For  
 223 small values of  $P_s$ , self-oscillations cannot be triggered and, as mentioned before, the masses stop after some  
 224 initial transients. However, when the pressure overcomes a threshold value close to  $P_s \approx 0.0056$ , a Hopf  
 225 bifurcation occurs and a limit cycle is established. The oscillations increase their amplitude as  $P_s$  augments,

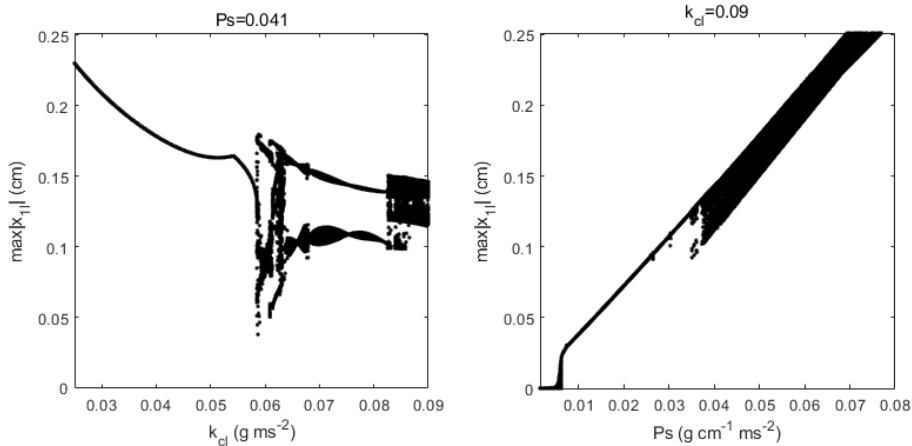


Figure 4: Left subfigure: bifurcation plot for fixed  $P_s = 0.041$  and varying stiffness coupling between masses from  $k_{cl} = 0.025$  to  $k_{cl} = 0.09$ . Right subfigure: bifurcation plot for fixed  $k_{cl} = 0.09$  and varying subglottal pressure from  $P_s = 0.015$  to  $P_s = 0.08$ .

226 but once reached another limit value of  $P_s \approx 0.0377$  they become chaotic. The right subfigure of Fig. 4  
 227 clearly exposes the process by which the three regimes previously shown in Fig. 2 develop.

228 Our goal in this paper is to determine whether it would be possible to establish some chaos controlling  
 229 mechanism so that the results in the third row of Fig. 2 could look like those in the second row, and the  
 230 phase space top-right subfigure in Fig. 3 for the volume flow velocity could be like the top-left one, even  
 231 when the subglottal pressure is high. As said in the introduction of the paper, rather than trying to control  
 232 the system by means of some external force, we aim to do so by attaching some kind of smart material to  
 233 the vocal folds and modify their effective mechanical properties.

#### 234 4. Controlling the chaotic motion of the vocal folds

##### 235 4.1. Chaos control by altering the system energy through external forces

Let us next summarize the basics of the chaos control approach proposed in [41–43] and adapt it to the problem at hand. The key idea in those works is to either increase or lower the overall energy of the system to a value in which the system gets stabilized. For instance, if a change in a system parameter leads to a period-doubling bifurcation, its energy would typically grow as sub-harmonics would contribute to the fundamental frequency [41]. The sum of kinetic and potential energy of the vocal folds is given by

$$E = \frac{1}{2} \mathbf{v}^\top \mathbf{M} \mathbf{v} + \frac{1}{2} \mathbf{x}^\top \mathbf{K} \mathbf{x}, \quad (6)$$

which once averaged over time  $T$  becomes

$$\langle E \rangle = \frac{1}{T} \int_0^T \left( \frac{1}{2} \mathbf{v}^\top \mathbf{M} \mathbf{v} + \frac{1}{2} \mathbf{x}^\top \mathbf{K} \mathbf{x} \right) dt. \quad (7)$$

If the system dynamics is periodic,  $T$  would correspond to its period, while if it is chaotic  $T \rightarrow \infty$ . The rate of energy change of the system is obtained from the time derivative of Eq. (6), taking into account that all involved block matrices in the first row of Eq. (4) are symmetric,

$$\dot{E} = \mathbf{v}^\top (\mathbf{M} \dot{\mathbf{v}} + \mathbf{K} \mathbf{x}) = \mathbf{v}^\top [-\mathbf{C} \mathbf{v} - \Theta(\mathbf{x}) \mathbf{x} + \mathbf{f}_v(\mathbf{x})] \quad (8)$$

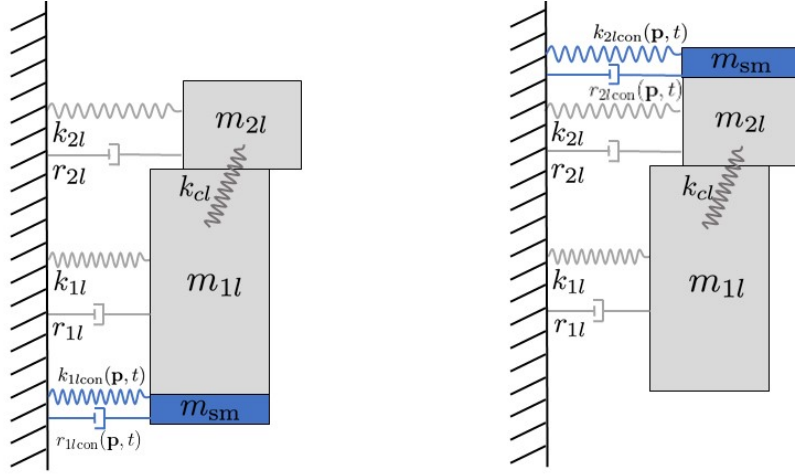


Figure 5: Attaching a smart material to mass  $m_{1l}$  (left column) or to mass  $m_{2l}$  (right column). The damping  $r_{il\text{con}}(\mathbf{p}, t)$  and stiffness  $k_{il\text{con}}(\mathbf{p}, t)$  can depend on variables such as  $\mathbf{p} = \{\mathbf{x}, \mathbf{v}, U\}$  and time, and be tuned so as to suppress the chaotic motion of the vocal folds.

The control strategy in [41] essentially consists in adding a control force to Eq. (8) typically depending on the velocity and in some cases on position, namely  $\mathbf{f}_c(\mathbf{v}, \mathbf{x})$ , so that this equation becomes

$$\dot{\mathbf{E}} = \mathbf{v}^\top (\mathbf{M}\dot{\mathbf{v}} + \mathbf{K}\mathbf{x}) = \mathbf{v}^\top [-\mathbf{C}\mathbf{v} - \mathbf{\Theta}(\mathbf{x})\mathbf{x} + \mathbf{f}_v(\mathbf{x}) + \mathbf{f}_c(\mathbf{v}, \mathbf{x})], \quad (9)$$

and the control force is such that the power  $\mathbf{v}^\top \mathbf{f}_c(\mathbf{v}, \mathbf{x})$  is either strictly positive or negative. This means that the control force will help increasing or decreasing the average system energy in Eq. (7), depending on the remaining non-linear components response to that change. The underlying idea is that the energy shift helps transitioning the system chaotic dynamics to periodic or quasiperiodic ones. Taking  $\mathbf{f}_c(\mathbf{v})$ , i.e., solely depending on the velocity  $\mathbf{v}$  (typically a linear dependence suffices) has proved useful in stabilizing one dimensional non-linear systems like the Van der Pol and Duffing oscillators, as well as controlling systems with impact forces [41–43]. As said in the introduction of this manuscript, the strategy has also revealed efficient for the case of networks of oscillators with some non-linear terms [41, 42]. Hence, one would expect the method to be effective for our vocal fold dynamics that involves two masses driven by flow pressure, which impact during their motion, closing the glottis. The option of taking  $\mathbf{f}_c(\mathbf{x})$ , i.e., a control force solely depending on the displacement  $\mathbf{x}$  will be also considered in forthcoming sections, in addition to  $\mathbf{f}_c(\mathbf{v})$ . But, as explained before, instead of thinking about applying external control forces we will rather integrate them in the system and think in terms of attaching a smart material to the vocal folds whose intrinsic parameters can be modified.

#### 4.2. Controlling the vocal folds with smart materials

In the case of the human vocal folds, adding an external control force  $\mathbf{f}_c(\mathbf{v}, \mathbf{x})$  to the force vector  $\mathbf{f}_v$  is not feasible. At most one could think of varying the vocal folds tension by stimulating the nerves driving them. As exposed in the introduction of the paper, this is at the basis of the few existent vocal fold pacemakers oriented at abduction and respiratory problems, but this approach would not work if the involved nerves were seriously damaged. The alternative we start exploring in this paper is whether it would be possible to control the chaotic motion of the vocal folds by somehow attaching a smart material either to  $m_{1l}$  or to  $m_{2l}$ , such that its stiffness and/or damping could be modified at convenience. The situation is schematically depicted in Fig. 5, where in the left column the smart material is added to  $m_{1l}$ , while in the right column is glued to  $m_{2l}$ . The material has mass  $m_{\text{sm}}$  and will slightly elongate the glottis in a small quantity  $\Delta L$ . Although these aspects could be easily incorporated in the model of Eq. (4), we will assume them negligible

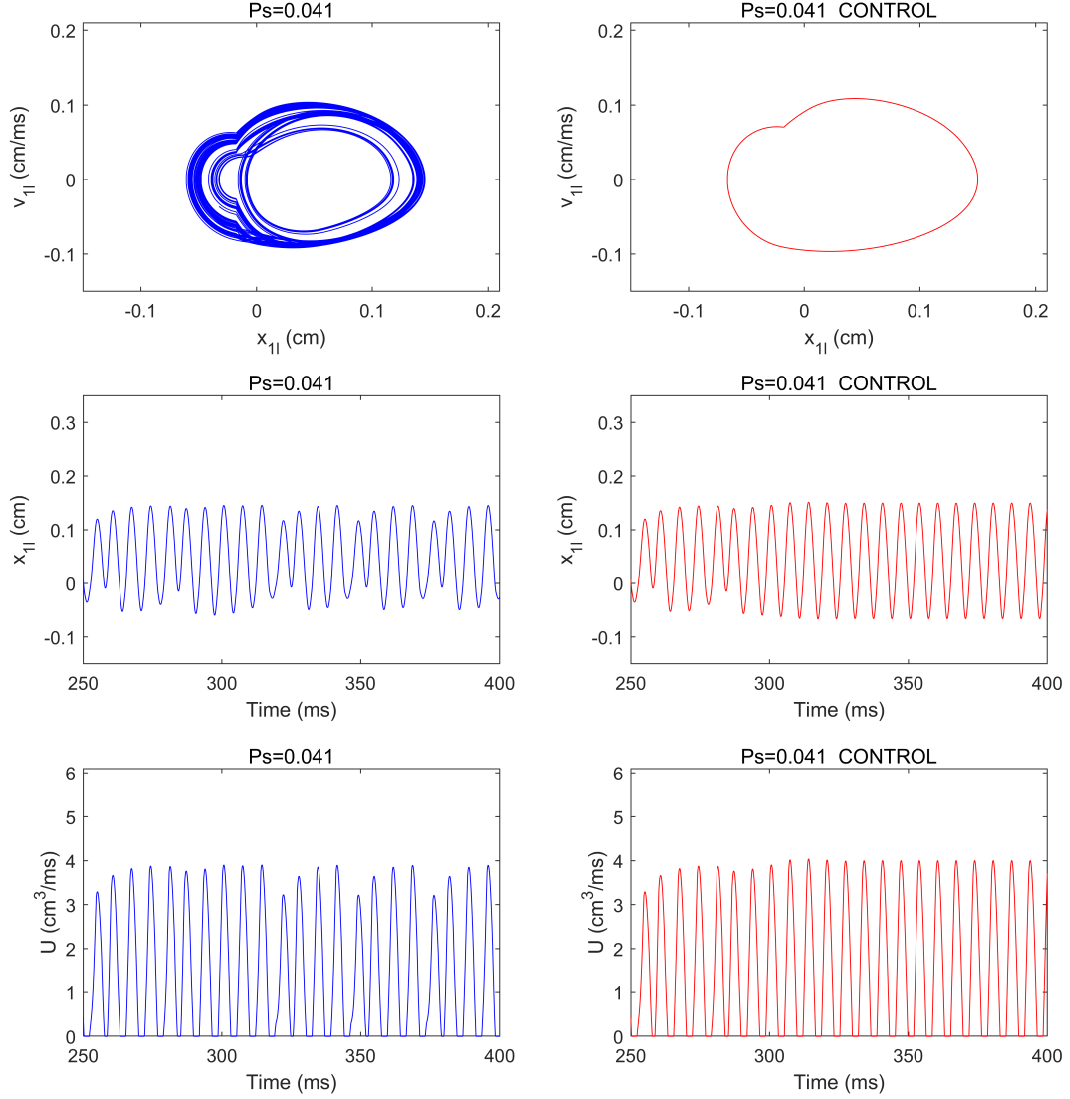


Figure 6: Control by modifying the damping  $r_{1l}$  of mass  $m_{1l}$ . First column: system with no control. Second column: system with control. Damping activated at  $t = 300$ . First row: phase space attractor ( $v_{1l}, x_{1l}$ ). Second row: time evolution of the displacement  $x_{1l}$ . Third row: time evolution of the glottal volume flow velocity. Results for a subglottal pressure of  $P_s = 0.041$ .

261 for simplicity in forthcoming simulations (i.e. we consider  $m_{sm} \ll m_{2l}, m_{1l}$  and  $\Delta L \ll L$ ). The focus  
 262 will be placed on finding appropriate laws for the varying smart material damping,  $c_{ilcon}(\mathbf{p}, t)$  and stiffness  
 263  $k_{ilcon}(\mathbf{p}, t)$ ,  $i = 1, 2$ , which may depend on variables  $\mathbf{p} = \{\mathbf{x}, \mathbf{v}, U\}$  and time. As will be seen, most of the  
 264 forthcoming work will concentrate on tuning the smart material damping to get an overall effective damping  
 265 that suppresses the vocal folds chaotic motion. A final section on stiffness control will also be provided,  
 266 though, as well as a brief discussion on the potential of current smart materials to attain our goal. Our  
 267 exploration will be limited to the simple two-mass model in Eq. (4).

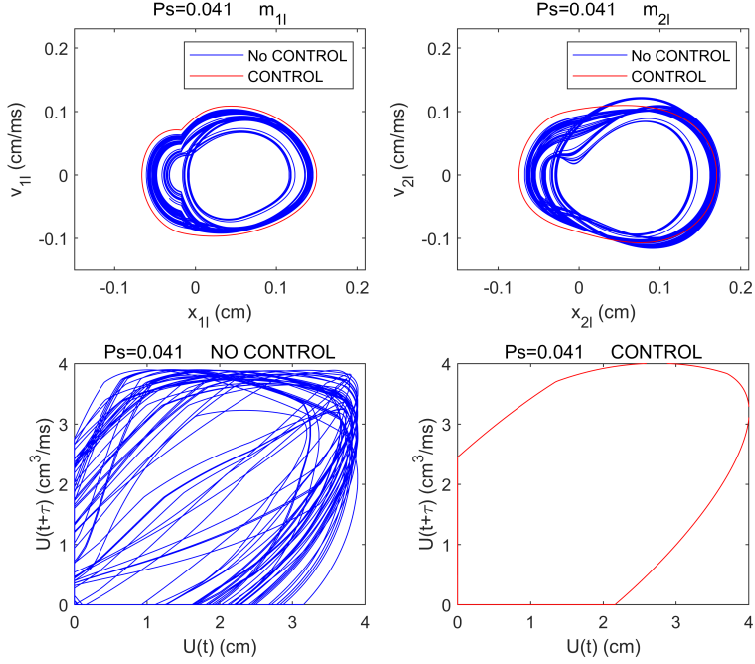


Figure 7: First row: attractors and period-1 orbit for the system with (red) and without (blue) damping control  $r_{1lcon}$ . Left: phase space  $(v_{1l}, x_{1l})$ , right: phase space  $(v_{2l}, x_{2l})$ . Second row: phase space plot for the glottal volume velocity  $U(t+\tau)$  versus  $U(t)$  without control (left) and with control (right). Results for a subglottal pressure of  $P_s = 0.041$ .

Instead of adding  $\mathbf{f}_c(\mathbf{v}, \mathbf{x})$  to the force vector in Eq. (4), our smart material attempt is in fact equivalent to moving this term to the l.h.s of the equation so that the practical consequence is that of modifying the stiffness and/or damping matrices in  $\mathbf{A}(\mathbf{y})$ , by adding some control to them. In other words, we look for the effects of changing

$$\mathbf{C} \longrightarrow \mathbf{C} + \mathbf{C}_c(\mathbf{v}, \mathbf{x}, U, t), \quad (10)$$

and/or

$$\mathbf{K} \longrightarrow \mathbf{K} + \mathbf{K}_c(\mathbf{v}, \mathbf{x}, U, t), \quad (11)$$

where  $\mathbf{C}_c$  and  $\mathbf{K}_c$  refer to the damping and stiffness control matrices provided by the smart material. It is important to note here, that one does not need to alter all damping or stiffness entries in  $\mathbf{C}$  and  $\mathbf{K}$ . The good news are that usually  $\mathbf{C}_c$  and  $\mathbf{K}_c$  will only have a single element different from zero. That is, modifying a single parameter suffices to stabilize the whole system. Before proceeding any further, it should be noticed that there is a trivial modification that could render the system stable. We know from the analysis in section 3 that setting the coupling stiffness to  $k_{cl} = 0.09$  instead of the standard value of  $k_{cl} = 0.025$  (see [5, 29]) triggers chaotic motion beyond a certain threshold subglottal pressure value. Recovering the value of  $k_{cl} = 0.025$  would result in periodic motion of the vocal folds. Nevertheless, the challenge here is to see if that motion can be restored through other parameter modifications rather than  $k_{cl}$ .

#### 4.2.1. Damping control

We start with one of the simplest possible options, which consists in altering the damping of the largest mass in the system, namely  $m_{1l}$ . This corresponds to taking a force  $\mathbf{f}_c(\mathbf{v}) = \mathbf{C}_c \mathbf{v}$  that is integrated in the modified damping matrix of the system as follows,

$$\mathbf{C} = \text{diag}(r_{1l}, r_{2l}) \longrightarrow \mathbf{C} + \mathbf{C}_c = \text{diag}(r_{1l} + r_{1lcon}, r_{2l}), \quad (12)$$

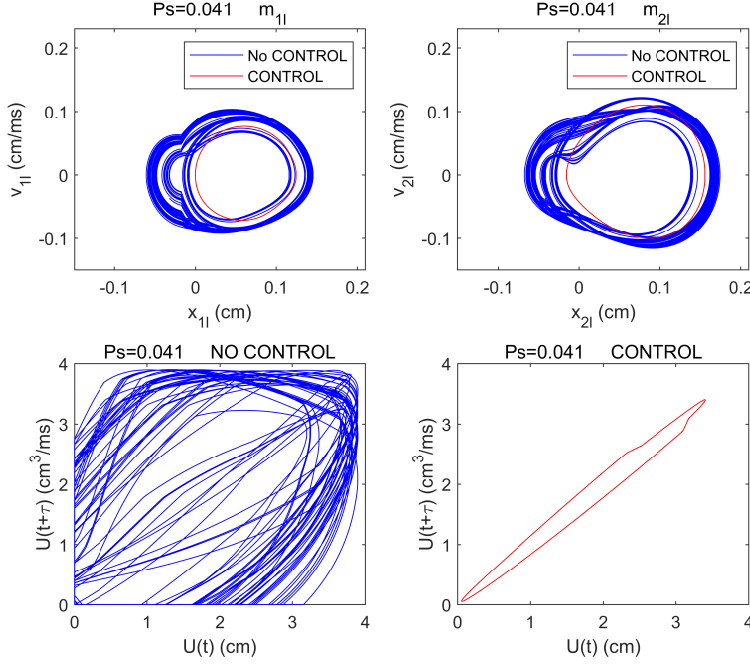


Figure 8: First row: attractors and period-1 orbits for the system with (red) and without (blue) damping control  $r_{2lcon}$ . Left: phase space  $(v_{1l}, x_{1l})$ , right: phase space  $(v_{2l}, x_{2l})$ . Second row: phase space plot for the glottal volume velocity  $U(t+\tau)$  versus  $U(t)$  without control (left) and with control (right). Results for a subglottal pressure of  $P_s = 0.041$ .

278 with  $|r_{1lcon}| < |r_{1l}|$ . Let us consider the case of a subglottal pressure of  $P_s = 0.041$  like in the last row of  
 279 Fig. 2 and take a small control value  $r_{1lcon} = -0.1r_{1l}$ . Initially, we let the system evolve without control and  
 280 when  $t = 300$  we activate the new smaller damping. This results in a slight increase of the system average  
 281 energy in Eq. (7), from  $\langle E \rangle = 6.12 \times 10^{-4}$  to  $\langle E_{con} \rangle = 7.68 \times 10^{-4}$ . The effects of diminishing the damping  
 282 are plotted in Fig. 6. The first column in the figure corresponds to the results of the simulations without  
 283 control, while the second column contains those with control. In the first row we observe how the strange  
 284 attractor transforms to a cycle for the new damping value. The data in these figures have been plotted  
 285 from  $t = 500$  to  $t = 1000$ . In the second row it is seen how the displacement  $x_{1l}$  becomes periodic beyond  
 286  $t = 300$ , once the control is triggered. Also, the volume flow velocity in the third row becomes regular  
 287 (compare it with the evolution of  $U$  in the last row of the first column), growing from zero, when the glottis  
 288 is closed, to its maximum value and then decreasing again until the next contact between masses takes  
 289 place. The time duration of the glottis closure remains constant when the control is activated. Very similar  
 290 results are obtained for the mass  $m_{2l}$  that will not be reproduced herein for brevity. To better appreciate  
 291 the stabilization effects of decrementing the damping of  $m_{1l}$ , in the first row of Fig. 7 we have plotted the  
 292 attractors in phase spaces  $(v_{1l}, x_{1l})$  and  $(v_{2l}, x_{2l})$  when no damping modification is applied (blue lines) and  
 293 the closed orbits (red lines) achieved when  $r_{1lcon}$  is triggered. In the second row of the figure we make use  
 294 again of Takens's theorem and plot  $U(t+\tau)$  against  $U(t)$  to show how the strange attractor in the left figure  
 295 gets stabilized through damping in the right figure. The glottal flow volume velocity, which is our final most  
 296 important variable for voice generation has therefore acquired the right shape.

Next, we may wonder what happens if instead of acting on the damping,  $r_{1l}$ , of the first mass, we act  
 on  $r_{2l}$  of the second mass,  $m_{2l}$ . That is, we now make the modification,

$$\mathbf{C} = \text{diag}(r_{1l}, r_{2l}), \longrightarrow \mathbf{C} + \mathbf{C}_c = \text{diag}(r_{1l}, r_{2l} + r_{2lcon}), \quad (13)$$

297 with  $|r_{2lcon}| < |r_{2l}|$ . The situation is now by far more tricky than when changing  $r_{1l}$ . The mass  $m_{2l}$  is

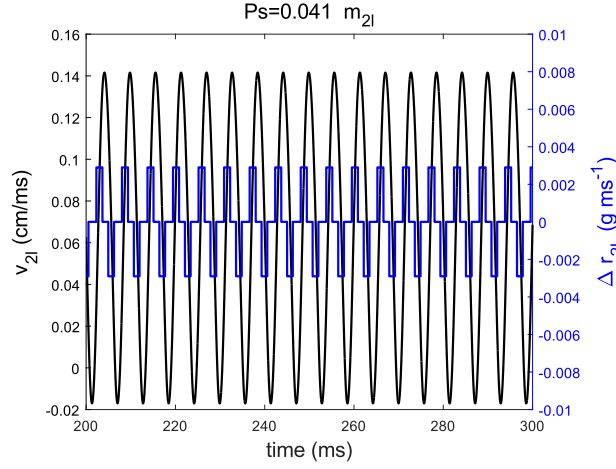


Figure 9: Dynamic damping modification  $r_{2l\text{con}} \text{sgn}(v_{2l})$  (blue line) depending on the velocity  $v_{2l}$  (black line) of the small mass  $m_{2l}$ .

298 twenty times smaller than  $m_{1l}$  and acting on it to control the whole dynamics of the system through  $r_{2l}$   
 299 is problematic. To begin with, testing  $r_{2l\text{con}} = -0.1r_{2l}$  is not enough to stabilize the system and a higher  
 300 percentage of variation of  $r_{2l}$  is required. Periodicity is attained when  $r_{2l\text{con}} \sim -0.25r_{2l}$ , but there is a  
 301 problem associated to it. The time duration of the vocal folds contact is negligible and for slightly higher  
 302 values of  $r_{2l\text{con}}$ , namely  $\sim -0.29r_{2l}$ , it simply disappears. This means that while the glottal volume velocity

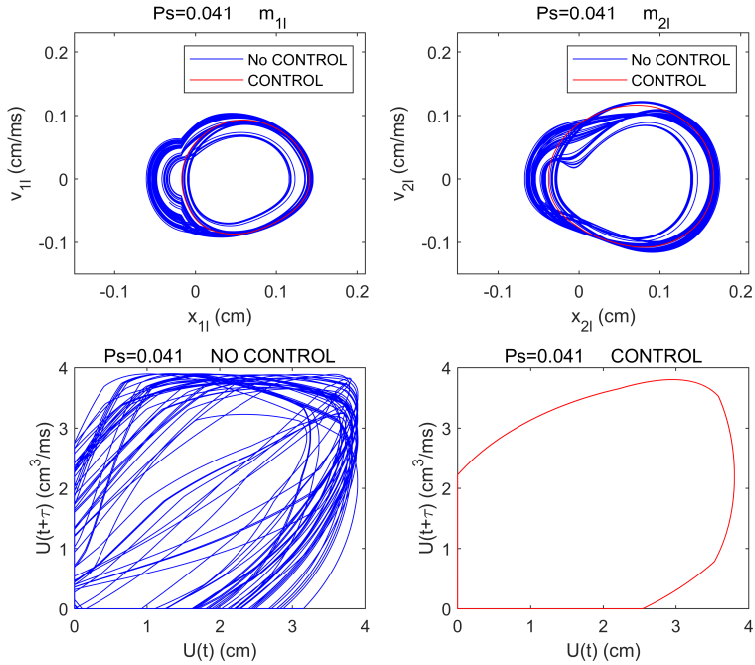


Figure 10: First row: attractors and period-1 orbits for the system with (red) and without (blue) damping control  $r_{2l} + r_{2l\text{con}} \text{sgn}(v_{2l})$ . Left: phase space  $(v_{1l}, x_{1l})$ , right: phase space  $(v_{2l}, x_{2l})$ . Second row: phase space plot for the glottal volume velocity  $U(t + \tau)$  versus  $U(t)$  without control (left) and with control (right). Results for a subglottal pressure of  $P_s = 0.041$ .

303  $U$  will be pulsating, it would never be zero, giving place to a breathy voice which is undesirable. The  
 304 problem is clearly illustrated in Fig. 8 that shows equivalent subplots to the previous ones in Fig. 7. As  
 305 observed in the first row, the motion of the two masses gets stabilized and two period-1 cycles clearly form.  
 306 However, when we look at the volume velocity in the second row (bottom-right figure), it becomes apparent  
 307 that its corresponding closed orbit does not cross the axes so the breathy effect will clearly manifest. In  
 308 this case, the system average energy has decreased from  $\langle E \rangle = 6.12 \times 10^{-4}$  to  $\langle E_{\text{con}} \rangle = 5.9 \times 10^{-4}$ . One  
 309 may conclude that acting on the first vocal fold mass is clearly an easier way to get an acceptable glottal  
 310 flow if damping changes are to be implemented (one could also consider changing both damping values  
 311 simultaneously, though it would clearly be better to find a strategy involving as less control parameters as  
 312 possible).

A more robust option than simply shifting  $r_{1l}$  or  $r_{2l}$  to new values is that of proposing a damping variation depending on the sign of the mass velocities. Following [41–43], we take

$$\mathbf{C} = \text{diag}(r_{1l}, r_{2l}) \longrightarrow \mathbf{C} + \mathbf{C}_c = \text{diag}(r_{1l} + r_{1l\text{con}} \text{sgn}(v_{1l}), r_{2l}), \quad (14)$$

or, alternatively,

$$\mathbf{C} = \text{diag}(r_{1l}, r_{2l}) \longrightarrow \mathbf{C} + \mathbf{C}_c = \text{diag}(r_{1l}, r_{2l} + r_{2l\text{con}} \text{sgn}(v_{2l})), \quad (15)$$

313 with  $|r_{i\text{con}} \text{sgn}(v_{il})| < |r_{il}|$ ,  $i = 1, 2$ . This obviously implies that one should be able to change the damping  
 314 of the smart material attached to the vocal folds very rapidly, at least twice per oscillation. This is a real  
 315 challenge for current smart materials (see the discussion in section 4.2.4). Here, the main difference with the  
 316 previous proposals is that the amount of increased damping depends on the sign of the mass velocity. Let us  
 317 focus on the second mass, for which severe problems were found when just changing the value of  $r_{2l}$  to a new  
 318 one. We implement the time varying damping depicted in Fig. 9, according to the general strategy in [42].  
 319 As observed in the figure, when the velocity  $v_{2l}$  augments  $r_{2l\text{con}}$  helps increasing the original damping  $r_{2l}$ ,  
 320 while it diminishes it when the opposite occurs. The effects of such variations are remarkable. Analogous  
 321 results to those of Fig. 8 are plotted in Fig. 10, using the new dynamic damping law of Eq. (15). The  
 322 improvement is striking. The contact between vocal folds is similar to that obtained when we acted on  
 323 the first mass and  $U$  becomes totally regular again. With this approach, the average energy of the system  
 324 slightly increases from  $\langle E \rangle = 6.12 \times 10^{-4}$  to  $\langle E_{\text{con}} \rangle = 6.79 \times 10^{-4}$ .

#### 325 4.2.2. Damping control with volume velocity feedback for varying subglottal pressure

326 Up to now, the suggested damping strategies for controlling the chaotic motion of the vocal folds have  
 327 been presented for a fixed value of the subglottal pressure, namely  $P_s = 0.041$ . However, in practice  $P_s$  will  
 328 rarely be constant and can exhibit significant differences during phonation. Therefore, it would be highly  
 329 recommendable to have some type of feedback mechanism that could adapt the damping of the system to  
 330 subglottal pressure variations. That is the topic of this subsection.

331 To address the problem, we consider the subglottal pressure evolution plotted in the first row of Fig. 11.  
 332 As seen,  $P_s$  is taken constant and equal to 0.041 for the first 300 ms of the simulation, and then starts  
 333 growing following a parabolic profile up to a maximum of  $P_{s,\text{max}} = 0.08$ . Once passed the maximum, the  
 334 subglottal pressure diminishes and recovers its original value of  $P_s = 0.041$  at  $t = 1300$ . In the second row  
 335 of Fig. 11 we add 10% of normally distributed noise to  $P_s$  to check the robustness of the feedback strategy  
 336 to be presented below.

The basic idea for controlling the vocal fold oscillations for varying  $P_s$  consists in introducing a feedback mechanism that increases or decreases the system damping depending on the effects that the evolution of  $P_s$  has on the glottal volume velocity  $U$ . We consider the following strategy for the damping of the second mass,

$$\mathbf{C} = \text{diag}(r_{1l}, r_{2l}) \longrightarrow \mathbf{C} + \mathbf{C}_c = \text{diag}(r_{1l}, r_{2l} + [r_{2l\text{con}} + \Delta r_{2l\text{con}}(U(t', t'' \dots t^N))] \text{sgn}(v_{2l})). \quad (16)$$

337 As compared to Eq. (15), at time  $t$  of the system evolution the damping value is not only modified according  
 338 to the sign of the velocity  $v_{2l}$  of the second mass  $m_{2l}$ , but also by a new term,  $\Delta r_{2l\text{con}}(U(t', t'' \dots t^N))$ ,

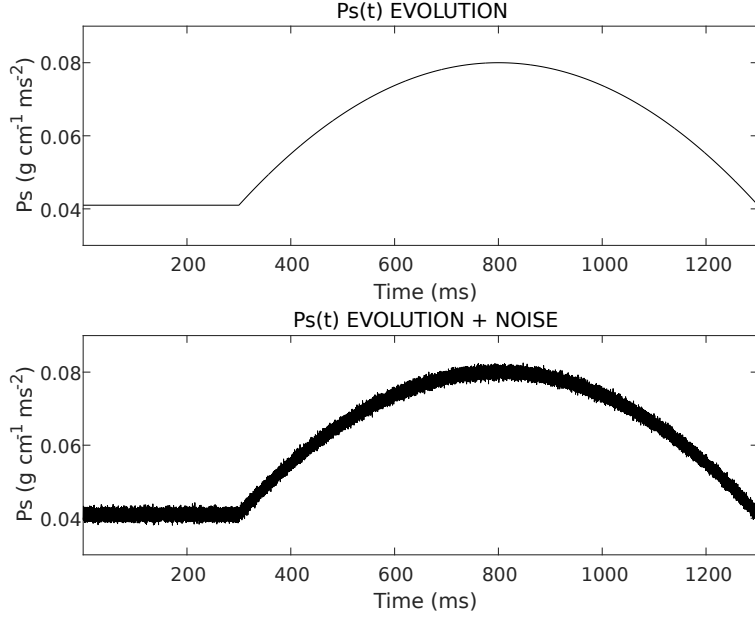


Figure 11: Subglottal pressure evolution. **Top row:**  $P_s$  remains constant for the first 300 ms, then increases following a parabolic profile up to a maximum of  $P_{s,\text{max}} = 0.08$  and recovers its original value for  $t = 1300$  ms. **Bottom row:**  $P_s$  exhibits the same time evolution of the top row but with a 10% of normally distributed noise.

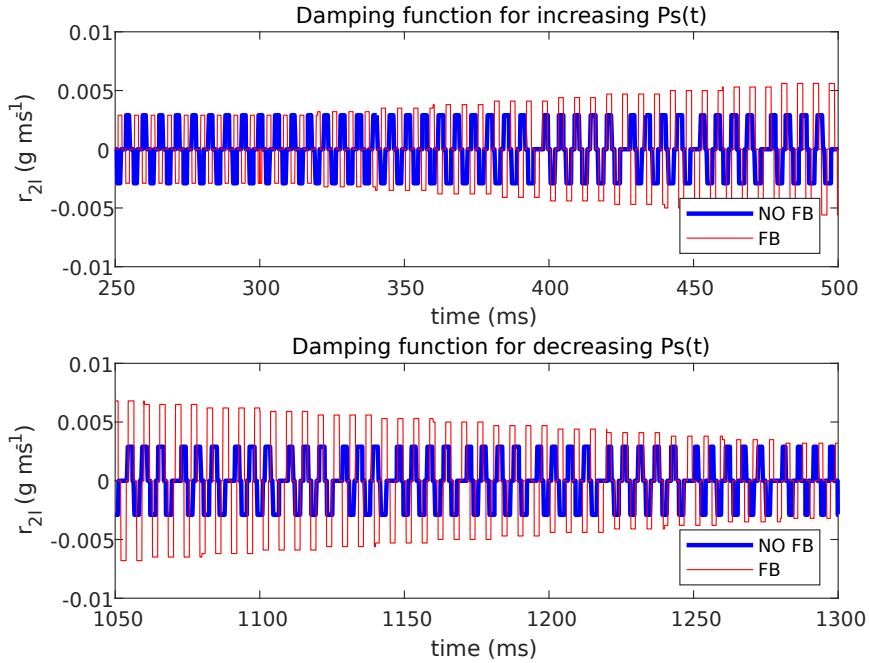


Figure 12: Comparison between the dynamic damping control without  $U$  feedback,  $r_{2l\text{con}} \text{sgn}(v_{2l})$  (blue line), and with  $U$  feedback  $[r_{2l\text{con}} + \Delta r_{2l\text{con}}(U(t', t'' \dots t^N))] \text{sgn}(v_{2l})$  (red line), when the subglottal pressure  $P_s$  starts growing according to the parabolic profile in Fig. 11 (top row), and when it gets back to its original value (bottom row).

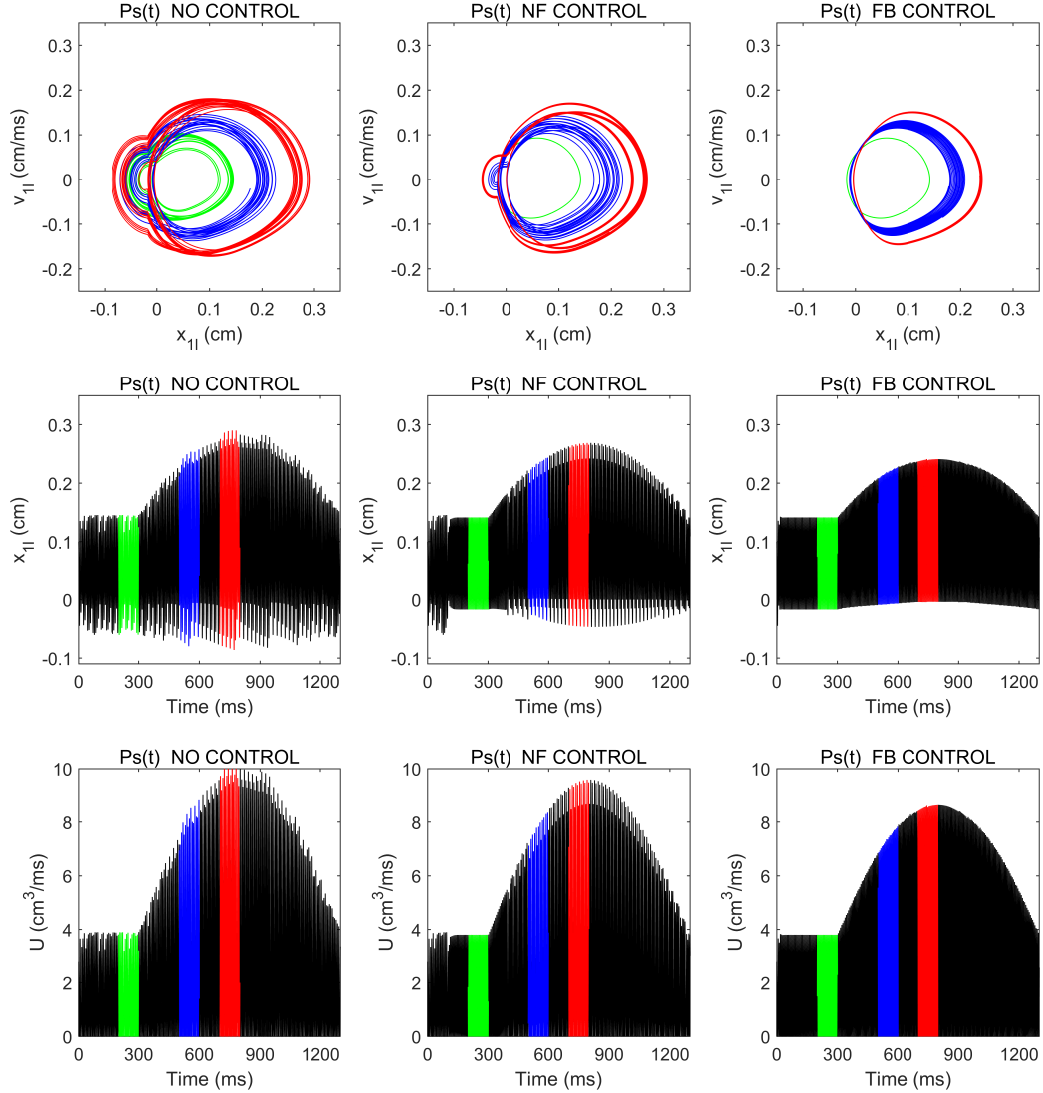


Figure 13: Comparison of damping control strategies when  $P_s$  evolves according to the top row of Fig. 11. First column: no control. Second column: damping control in Eq. (15). Third column: damping control with  $U$  feedback in Eq. (16). The NF control is activated for  $t \geq 100$  ms and the FB one for  $t \geq 300$  ms. First row: phase space trajectories corresponding to the coloured time interval stripes in the second row. Second row: evolution of the first mass displacement  $x_{1l}$ . Third row: evolution of the glottal volume velocity  $U$ .

339 which depends on previous time values  $t', t'' \dots t^N$  of the glottal volume velocity  $U$ .  $\Delta r_{2lcon}(U(t', t'' \dots t^N))$   
340 is computed as follows. It is first assigned a zero value. As the system evolves, every 20 ms we find the  
341 peaks of  $U$  in the preceding 30 ms and compute a linear regression for them. Usually four to five peaks are  
342 found,  $U_{pk,i}$ ,  $i = 1 \dots 4, 5$ . If the resulting slope is positive and the absolute value of the difference between  
343 the maximum and minimum peaks of  $U$  exceeds a threshold value  $U_{tol} = 0.1$ , i.e.  $|U_{pk,max} - U_{pk,min}| > U_{tol}$   
344 we take  $\Delta r_{2lcon}(U(t', t'' \dots t^N)) = 3 \times 10^{-4}$  and the damping control increases. If  $|U_{pk,max} - U_{pk,min}| > U_{tol}$

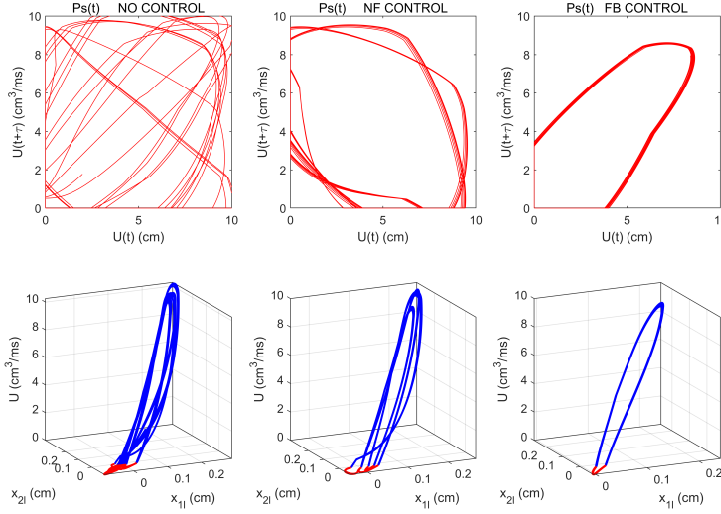


Figure 14: First row: phase space trajectories for the glottal volume velocity  $U(t+\tau)$  versus  $U(t)$  in the time interval  $[700, 800]$  ms (red stripe in Fig. 13) for the cases of no control, damping control for constant  $P_s$  in Eq. (15) and damping control with  $U$  feedback for varying  $P_s$  in Eq. (16). Second row: plots of  $U(x_{1l}, x_{2l})$  for the same time interval. The red colour indicates zero values for  $U$  which occurs whenever the left and right masses contact.

345 but the slope is negative then  $\Delta r_{2lcon}(U(t', t'' \dots t^N)) = -3 \times 10^{-4}$  and the control damping diminishes. If  
346  $|U_{pk,max} - U_{pk,min}| < U_{tol}$  no modification is made. The difference between the control damping computed  
347 according to Eq. (15) and to Eq. (16) is shown in Fig. 12. The first row in the figure presents the evolution  
348 of  $r_{2lcon} \operatorname{sgn}(v_{2l})$  (blue line) and of  $[r_{2lcon} + \Delta r_{2lcon}(U(t', t'' \dots t^N))] \operatorname{sgn}(v_{2l})$  (red line) between  $t = 250$  and  
349  $t = 500$ , when the subglottal pressure starts augmenting (see Fig. 11). As observed, the damping with  $U$   
350 feedback control increases with  $P_s$ , while that without control remains unaltered. In the second row of the  
351 figure, we depict the control damping evolution between  $t = 1050$  and  $t = 1300$ , when  $P_s$  diminishes to its  
352 original value  $P_s = 0.041$ . As seen in the figure, the damping with  $U$  feedback control (red line) progressively  
353 diminishes until it recovers that computed without  $U$  feedback (blue line). In the case of a more abrupt  
354 and complex time evolution of  $P_s$  than that in Fig. 11, one could think of designing alternative feedback  
355 strategies if the proposed one was not sufficient.

356 The effectiveness of the  $U$  feedback damping control strategy on the vocal folds behaviour is shown in  
357 Fig. 13. The first column in the figure corresponds to the case in which no control is applied to the system.  
358 The second column contains the results for the constant damping control strategy without  $U$  feedback in  
359 Eq. (15), and the third column shows the results when the  $U$  feedback control of Eq. (16) is considered. The  
360 constant control strategy is activated for  $t \geq 100$  ms and the  $U$  feedback one for  $t \geq 300$  ms. As regards  
361 the row by row results in the figure, let us focus on the second row contents before commenting on the first  
362 one. The second row of the figure presents the evolution of  $x_{1l}$  with time for a total of 1300 ms, during  
363 which  $P_s$  varies according to the top row of Fig. 11. As we have decided to plot the entire time interval,  
364 individual oscillations are hardly visible. However, one can perceive from the first subfigure in the second  
365 row that the lack of control leads to strong chaotic motion, while this is slightly smoothed when applying  
366 the damping control without  $U$  feedback, and definitely turned into periodic motion when implementing  
367 the  $U$  feedback control. To better distinguish such behaviour, we have depicted three coloured stripes in  
368 the figure, green, blue and red, which respectively cover the time intervals  $[200, 300]$  ms,  $[500, 600]$  ms and  
369  $[700, 800]$  ms. The phase space plots  $(v_{1l}, x_{1l})$  corresponding to these time intervals are presented in the first  
370 row of Fig. 13, using the same colour code. In the case of no control, the trajectories evolve into strange  
371 attractors of increasing amplitude as  $P_s$  augments, as one could have expected. When applying control  
372 without  $U$  feedback, it is seen that the motion becomes periodic for  $[200, 300]$  ms because for this interval

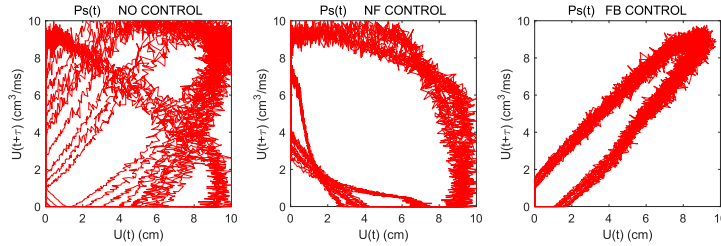


Figure 15: Phase space trajectories for the glottal volume velocity  $U(t + \tau)$  versus  $U(t)$  in the time interval  $[700, 800]$  ms (red stripe in Fig. 13) for the cases of no control, damping control in Eq. (15) and damping control with  $U$  feedback in Eq. (16) for varying  $P_s$  in the presence of noise (bottom row of Fig. 11).

373 the pressure still has constant value  $P_s = 0.041$ . Therefore a green cycle appears in the second subfigure  
 374 of the first row in Fig. 13. However, as  $P_s$  gets higher, the control is insufficient and the trajectories in  
 375 phase space (blue and red) soon become complex, departing from the desired periodic motion. As opposed,  
 376 when the  $U$  feedback is applied, all trajectories in phase space remain periodic. The same green cycle of  
 377 the previous subfigure is recovered and when the subglottal pressure is increased the motion does not loose  
 378 periodicity but simply increases its amplitude (see the blue and red lines). Finally, in the third row of Fig. 13  
 379 we have plotted the time evolution of the glottal volume velocity  $U$ . The same tendencies found for  $x_{1l}$  are  
 380 encountered for  $U$ , which seems to exhibit a totally regular behaviour as  $P_s$  grows if the  $U$  feedback control  
 381 is activated. Given that  $U$  is the variable of primary importance in this paper, we analyse it in some more  
 382 detail in Fig. 14.

383 The first row of Fig. 14, presents the trajectories in the phase space  $(\dot{U}, U)$  for the time interval  
 384  $[700, 800]$  ms (red stripe in Fig. 13) making use of Takens's theorem once more. As observed, and as  
 385 already shown in previous figures, the trajectories in the case of no control are totally chaotic, which results  
 386 in a very irregular pattern of  $U$  that would lead to critical problems for voice generation. When the control  
 387 of Eq. (15) is applied some improvement is observed. However, the closure of the vocal folds still has very  
 388 different durations (look at the zero values of the trajectories in the vertical and horizontal axes of the  
 389 second subfigure in the first row). This would result again in poor voice quality. We can see, though, that  
 390 the  $U$  feedback control is able to deal with the situation producing a very regular pattern for  $U$  that only  
 391 presents very slight variations of the contact duration and amplitude as  $P_s$  increases. Such behaviour can  
 392 also be appreciated plotting  $U$  against the position of the masses (second row of Fig. 14),  $x_{1l}$  and  $x_{2l}$ , as  
 393 we did in the second row of Fig. 3. The problems detected in the phase space trajectories clearly reflect in  
 394 the plots of  $U(x_{1l}, x_{2l})$ . It is remarkable how the  $U$  feedback control is able to stabilize the system so that  
 395  $U(x_{1l}, x_{2l})$  for  $P_s$  close to 0.08 essentially exhibits the same behaviour than for  $P_s = 0.021$  in Fig. 3, but  
 396 with a larger amplitude.

397 Finally, in Fig. 15, we check whether the presented controlling mechanisms are robust with respect to  
 398 noise perturbations. To that end we have applied the damping control strategy in Eq. (15) and that with  $U$   
 399 feedback in Eq. (16) to the subglottal pressure evolution in the bottom row of Fig. 11. As said, that figure  
 400 corresponds to  $P_s$  in the top row but with an addition of 10% of normally distributed noise. Therefore, we  
 401 want to check now if the proposed control strategies would be efficient in the demanding situation where  
 402 noise is added to a varying subglottal pressure. As observed in Fig. 15, where we have plotted the same  
 403 phase space plots  $(\dot{U}, U)$  than in the first row of Fig. 14, both control options turn to be quite robust to the  
 404 presence of noise and do not substantially alter their behaviour. Note that in the case of the  $U$  feedback  
 405 control (third column in Fig. 15) the results are quite neat and topologically resemble those in the first  
 406 row, third column of Fig. 14. That could lead to admissible self-sustained oscillations of the vocal folds and  
 407 proper glottal volume velocity generation as compared to control without feedback or no control at all. The  
 408 robustness under noise perturbations of damping control strategies based on altering the system energy was  
 409 also reported for impact problems in [43] and it is confirmed in the current example of voice phonation.

410 4.2.3. Stiffness control

Up to now, the chaos control strategies presented in this work have relied on modifying either the damping  $r_{1l}$  of the first mass  $m_{1l}$  or  $r_{2l}$  of  $m_{2l}$ . In this section, it will be shown that it is also possible to switch from chaotic oscillations to periodic ones by modifying the stiffness matrix of the system Eq. (4), instead of the damping one. We may consider the options of taking,

$$\mathbf{K} = \begin{pmatrix} k_{1l} + k_{cl} & -k_{cl} \\ -k_{cl} & k_{2l} + k_{cl} \end{pmatrix} \longrightarrow \mathbf{K} + \mathbf{K}_c = \begin{pmatrix} k_{1l} + k_{1l\text{con}} + k_{cl} & -k_{cl} \\ -k_{cl} & k_{2l} + k_{cl} \end{pmatrix} \quad (17)$$

or alternatively,

$$\mathbf{K} = \begin{pmatrix} k_{1l} + k_{cl} & -k_{cl} \\ -k_{cl} & k_{2l} + k_{cl} \end{pmatrix} \longrightarrow \mathbf{K} + \mathbf{K}_c = \begin{pmatrix} k_{1l} + k_{cl} & -k_{cl} \\ -k_{cl} & k_{2l} + k_{2l\text{con}} + k_{cl} \end{pmatrix}. \quad (18)$$

For the sake of brevity, and not to repeat the many tests carried out in the previous sections on damping control, we will restrain to the first option in Eq. (17) and deal with the case of constant subglottal pressure  $P_s = 0.041$ . In particular, we will modify the stiffness associated to the first mass in Eq. (17) according to the following law,

$$k_{1l} \longrightarrow k_{1l} + \Delta k_{1l\text{con}}(U(t)). \quad (19)$$

411 Here, the dependence of  $\Delta k_{1l\text{con}}(U(t))$  on the volume velocity  $U$  is such that if  $0 < U(t) \leq U_{\text{tol}}$  we set  
 412  $\Delta k_{1l\text{con}}(U(t)) = 0.75k_{1l}$ , otherwise we set  $\Delta k_{1l\text{con}}(U(t))$  to zero. A few numerical experiments have revealed  
 413 that taking  $U_{\text{tol}} = 1$  provides stabilization. The functioning of the stiffness control strategy is shown in  
 414 Fig. 16, where the evolution of  $U$  and  $\Delta k_{1l\text{con}}(U(t))$  are plotted for the interval [250, 400] ms. Note that the  
 415 control is activated at  $t = 300$  and a few milliseconds after that, namely beyond  $t = 350$ , the volume velocity  
 416 has already become totally regular. The efficiency of the stiffness control is more clearly shown in Fig. 17,  
 417 where, as in previous figures, we compare the results for the system with (second column) and without  
 418 control (first column). As clearly seen from the time evolution of  $x_{1l}$  and  $U$  (second and third rows) and the  
 419 trajectories in the phase space  $(v_{1l}, x_{1l})$  (first row), the stiffness control is totally capable to stabilize the  
 420 chaotic motion. Moreover, and as in previous tests with control damping laws, in Fig. 18 we have plotted  
 421 the phase space trajectories in  $(v_{1l}, x_{1l})$  and  $(v_{2l}, x_{2l})$  when there is no control (blue lines) and when the  
 422 control is switched on (red lines). Both masses oscillate periodically. The results in the phase space  $(\dot{U}, U)$   
 423 also reveal the regularity of the volume velocity which is necessary to produce a normal, healthy voice.

424 Finally, it is to be noted that the proposed stiffness control requires rather high values of  $\Delta k_{1l\text{con}}$  (up to  
 425  $0.75k_{1l}$ ), in comparison to the relative increase of the damping value in previous sections. As regards the  
 426 system average energy, in this case it has slightly increased from  $\langle E \rangle = 6.12 \times 10^{-4}$  to  $\langle E_{\text{con}} \rangle = 6.44 \times 10^{-4}$ .

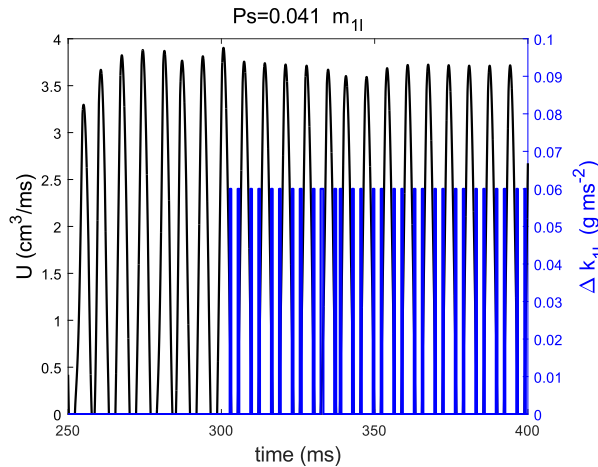


Figure 16: Dynamic stiffness modification  $\Delta k_{1l\text{con}}(U(t))$  (blue line) depending on the volume velocity  $U(t)$  (black line).

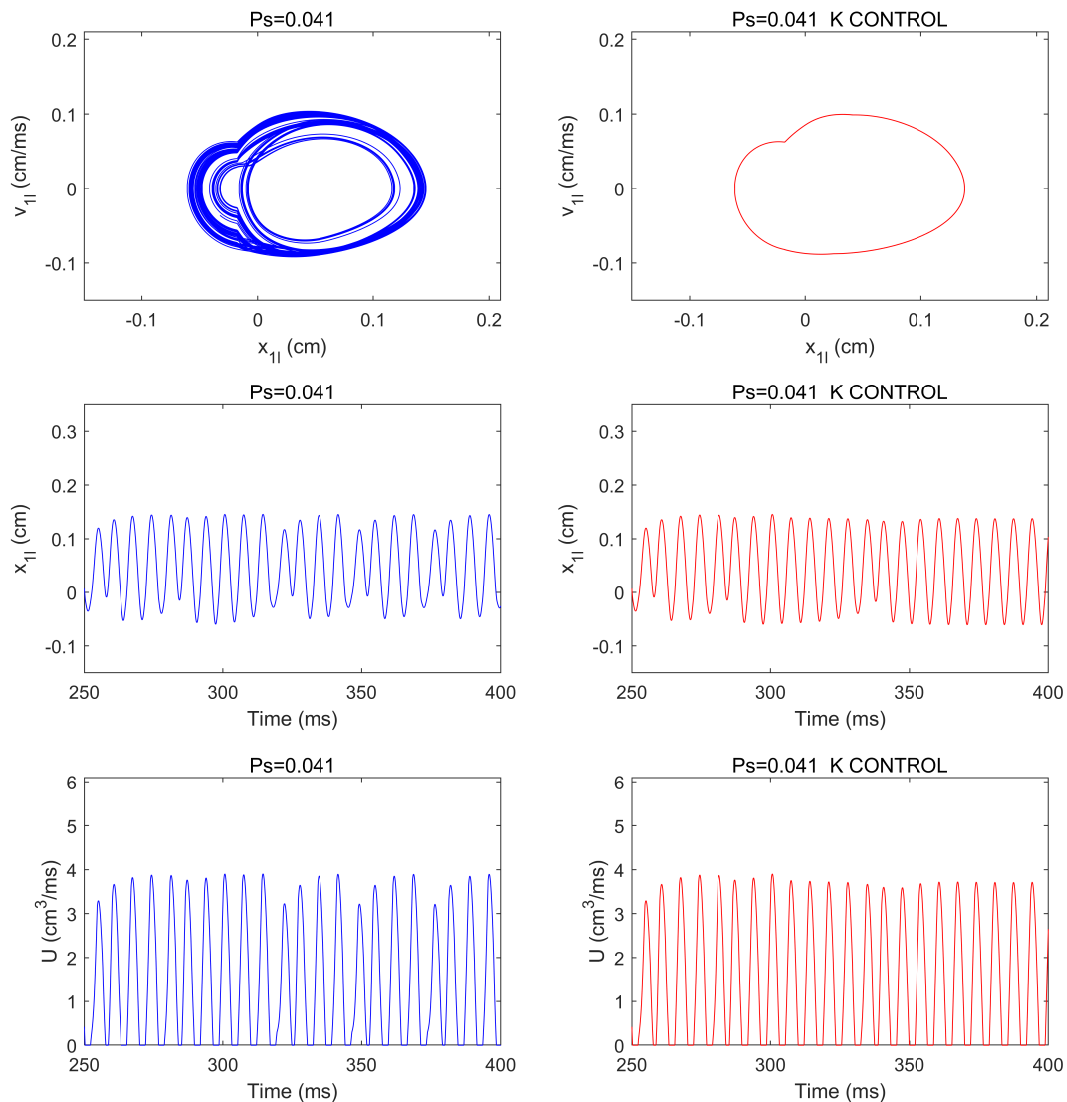


Figure 17: Control by modifying the stiffness  $k_{1l}$  of mass  $m_{1l}$ . First column: system without control. Second column: system with stiffness control, which is activated at  $t = 300$  ms. First row: phase space attractor  $(v_{1l}, x_{1l})$ . Second row: time evolution of the displacement  $x_{1l}$ . Third row: time evolution of the glottal volume flow velocity. Results for a subglottal pressure of  $P_s = 0.041$ .

#### 4.2.4. Brief discussion

In the preceding sections, we have proposed several options to control the chaotic oscillations of a two-mass model of the vocal folds and recover a proper glottal pulse for voice production. It is to be mentioned that the control of non-linear oscillators has been studied in detail in the past decades (see e.g. [51, 52]). The first attempts were devoted to single non-linear oscillators like the Duffing and the Van der Pol oscillators (among others), which respectively account for a cubic non-linear stiffness restoring force and a quadratic non-linear damping one. A wide range of strategies have proved useful for that purpose like the OGY

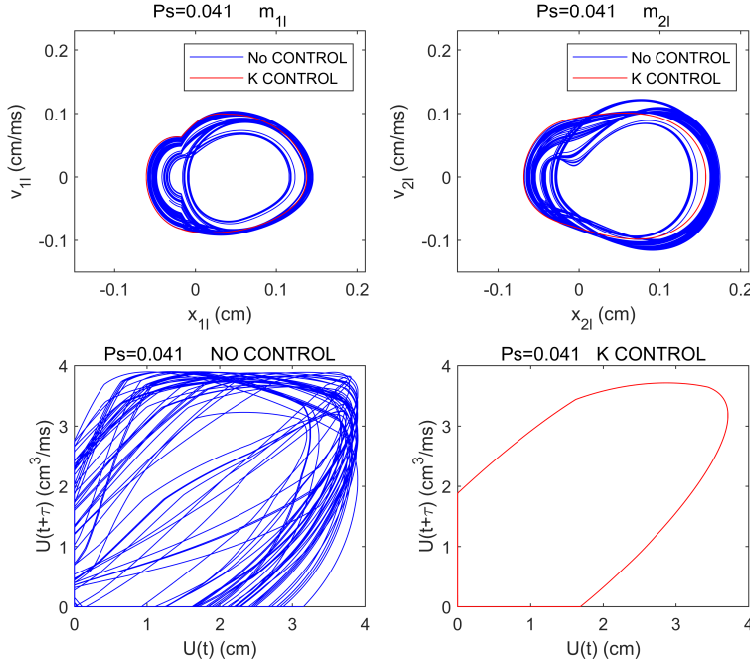


Figure 18: First row: attractors and period-1 orbit for the system with (red) and without (blue) stiffness control  $\Delta k_{1l\text{con}}(U(t))$ . Left: phase space  $(v_{1l}, x_{1l})$ , right: phase space  $(v_{2l}, x_{2l})$ . Second row: phase space plot for the glottal volume velocity  $U(t+\tau)$  versus  $U(t)$  without control (left) and with stiffness control (right). Results for a subglottal pressure of  $P_s = 0.041$ .

434 method [53], feedback strategies [54], non-linear adaptative approaches [55], modified linearization [56],  
 435 synchronization [57], control without feedback [58], or the altering energy method [41, 42] adopted in this  
 436 work. As mentioned in the introduction, several of these approaches are also effective when non-linearity  
 437 manifests because of impacts [37–40, 43, 59]. However, less articles exist on the control of systems of  
 438 oscillators describing lumped physical models [40, 60, 61], like the one in the current work. In [41, 42], it was  
 439 checked that the altering energy approach is also very effective for networks of oscillators. This has been  
 440 confirmed for the two-mass model in the previous sections, when applying the strategy (with variations) to  
 441 distinct situations. It is expected that similar results would follow for higher dimension models of the vocal  
 442 folds (e.g., that in [7]).

443 With the exception of the control without feedback in [58], which relies on the classical option of linking  
 444 a tuned absorption damper to control the oscillator (the lack of feedback may lead to robustness problems),  
 445 all other strategies in the above paragraph involve an external control force acting on the mechanical system.  
 446 As this would not be possible for the vocal cords, in the previous sections we have suggested and analyzed the  
 447 possibility of using ideal smart materials to control the oscillations of the vocal folds, and prevent abnormal  
 448 voice production. Obviously, there is a long pathway from the theoretical analysis with ideal simple models  
 449 carried out insofar to any potential real application. In addition to practical issues such as how to obtain  
 450 the time series where to apply the control strategy (e.g., by means of a thin film accelerometer placed at the  
 451 vocal cords), a critical aspect concerns whether smart materials exist with the capability of rapidly changing  
 452 their damping and/or stiffness values at the frequencies needed for chaotic vocal folds control. This is a  
 453 strong challenge for current smart materials. Besides, while a damping variation in a viscoelastic material  
 454 can be frequency-dependent as either the storage modulus and the loss modulus change with the frequency  
 455 of the applied load, a stiffness variation for an elastic material will mostly depend on geometry changes  
 456 rather than on variations in the elastic modulus, which is an intrinsic property of the material.

457 From the wide range of smart materials described in the literature [44], some look promising and will

458 be worth exploring in the future. For instance, the actuators or artificial muscles defined in [62] are a  
459 class of materials and devices that can reversibly contract, expand, or rotate as a response to an external  
460 stimulus. A recent review [63] discusses the mechanisms, limitations and challenges of several actuators  
461 including shape memory alloys, ionic-polymer/metal composites and dielectric elastomer actuators, whereas  
462 in [64] electroactivated polymers are described as actuators suitable for biomedical applications. A dynamic  
463 stimulus of the actuator, might produce a rapid damping or a stiffness variation and recent approaches to  
464 understand the mechanisms behind such behaviours have been reported in [65, 66].

## 465 5. Conclusions

466 In this paper we have suggested the idea of a voice pacemaker that could control chaotic oscillations  
467 of the vocal folds and revert them to periodic ones. That pacemaker could be built by attaching a smart  
468 material to the vocal cords, with the capability of having tunable time varying damping and stiffness values.  
469 For simplicity, the mass of the smart material has been assumed negligible as compared to those of the  
470 vocal folds. Simulations have been performed for a symmetric two-mass model in which oscillations become  
471 chaotic for excessive subglottal pressure.

472 In the two-mass model, each vocal cord is characterized by two masses, the lower one being twenty  
473 times bigger than the upper one. To begin with, it has been shown that, for a fixed value of the subglottal  
474 pressure, an effective control strategy based on altering the system energy consists in slightly diminish the  
475 damping of the biggest mass through the action of the smart material. This stabilizes the motion of the  
476 vocal folds, which becomes periodic and closes the glottis at regular time intervals. That can be clearly seen  
477 in phase space plots of the motion of the masses, as well as when applying Taken's theorem to visualize the  
478 glottal volume velocity in phase space. Remember that a regular glottal volume velocity pulse is the key for  
479 proper voice generation. The situation is more intricate if one attempts to control the upper mass of the  
480 vocal cords because reducing its damping does not suffice. The vocal fold oscillations can become periodic  
481 but they do not collide, i.e., the glottis does not close. This would lead to an undesirable breathy glottal  
482 volume velocity and abnormal voice production. A more complex damping law is therefore required to get  
483 an admissible glottal pulse if one wants to control the system through the upper mass instead of the lower  
484 one. The trick here is to supply additional damping depending on the sign of the velocity of the upper mass.  
485 In this way, one can recover a similar control to that achieved with the first mass.

486 On the other hand, in a realistic situation the subglottal pressure will be rarely constant but vary with  
487 time. It would be thus interesting to establish a feedback control strategy to deal with that circumstance.  
488 This has been done for the very demanding case of controlling the upper mass. For varying subglottal  
489 pressure, we do not only change the sign of the damping depending on the upper mass velocity but we also  
490 modify its amplitude depending on previous values of the glottal volume velocity. Again, the results have  
491 clearly shown the validity of this strategy and how periodicity is recovered yielding a regular glottal pulse  
492 for correct voice generation. Another interesting aspect is that in practice, the subglottal pressure will not  
493 only evolve with time but present noise perturbations. The feedback control has been also tested in such  
494 condition by adding a 10% of normally distributed noise to the subglottal pressure signal. It has been shown  
495 that the feedback control is noticeably robust to the presence of noise and that the resulting glottal pulses  
496 present admissible variations in amplitude and in the glottis closure time.

497 To finish the paper, we have considered the option of controlling the chaotic motion of the vocal folds  
498 by acting on the stiffness of the smart material instead of acting on its damping. For constant subglottal  
499 pressure, it has been proposed to modify the stiffness of the lower mass of the vocal folds depending on the  
500 value of the glottal volume velocity. If that exceeds a given tolerance value, the stiffness augments by a  
501 constant factor, while no change is made for smaller values than the threshold. Once more, time evolution  
502 and phase space plots for the mass motion and volume velocity have revealed the efficiency of the method.  
503 Therefore, stiffness control could be also an option and in future works it will be worth exploring whether  
504 it may be also reliable for varying and/or noisy subglottal pressure.

505 The work presented in this paper intends to open the door to new ways of dealing with pathological  
506 voice disorders. It is to be mentioned though, that our analysis has been carried out for a very simple two-  
507 mass model of the vocal folds. In forthcoming works, we will analyse the smart material control approach

508 for models involving lateral paralyses and polyps which break the symmetry of the current model and also  
509 introduce new types of non-linearities. It is expected that the type of chaos control strategy presented herein  
510 could well adapt to those more complex models and situations.

## 511 Acknowledgements

512 The first and fourth authors thank the support of the project FEMVoQ (PID2020-120441GB-I00-AEI-  
513 10.13039/501100011033) from the Spanish Ministerio de Ciencia e Innovación. The second author would  
514 like to acknowledge the Full3DTalkingHead project (ANR-20-CE23-0008-03) from l'Agence Nationale de la  
515 Recherche. The third author would like to thank the Catalan Government for the quality accreditation given  
516 to her research group DIOPMA (2017 SGR 0118). DIOPMA is certified agent TECNIO in the category of  
517 technology developers from the Government of Catalonia.

## 518 References

- 519 [1] J. Van den Berg, Myoelastic-aerodynamic theory of voice production, *J. Speech Hear. Res.* 1 (1958) 227–244.  
520 [2] I. Titze, *The Myoelastic Aerodynamic Theory of Phonation*, National Centre for Voice and Speech, Iowa City, 2006.  
521 [3] K. Ishizaka, J. Flanagan, Synthesis of voiced sounds from a two-mass model of the vocal cords, *Bell Syst. Tech. Journal*  
522 51 (1972) 1233–1268.  
523 [4] J. C. Lucero, Dynamics of the two-mass model of the vocal folds: Equilibria, bifurcations, and oscillation region, *J.*  
524 *Acoust. Soc. Am.* 94 (1993) 3104–3111.  
525 [5] I. Steinecke, H. Herzel, Bifurcations in an asymmetric vocal-fold model, *J. Acoust. Soc. Am.* 97 (1995) 1874–1884.  
526 [6] D. E. Sommer, B. D. Erath, M. Zanartu, S. D. Peterson, Corrected contact dynamics for the Steinecke and Herzel  
527 asymmetric two-mass model of the vocal folds, *J. Acoust. Soc. Am.* 132 (2012) EL271–EL276.  
528 [7] B. H. Story, I. R. Titze, Voice simulation with a body-cover model of the vocal folds, *J. Acoust. Soc. Am.* 97 (1995)  
529 1249–1260.  
530 [8] R. Laje, T. Gardner, G. Mindlin, Continuous model for vocal fold oscillations to study the effect of feedback, *Phys. Rev.*  
531 *E* 64 (2001) 056201.  
532 [9] Y. Zhang, J. J. Jiang, Chaotic vibrations of a vocal fold model with a unilateral polyp, *J. Acoust. Soc. Am.* 115 (2004)  
533 1266–1269.  
534 [10] B. D. Erath, M. Zanartu, K. C. Stewart, M. W. Plesniak, D. E. Sommer, S. D. Peterson, A review of lumped-element  
535 models of voiced speech, *Speech Commun.* 55 (2013) 667–690.  
536 [11] J. Cisonni, A. Van Hirtum, X. Pelorson, J. Lucero, The influence of geometrical and mechanical input parameters on  
537 theoretical models of phonation, *Acta Acust. united Ac.* 97 (2011) 291–302.  
538 [12] P. Luizard, X. Pelorson, Threshold of oscillation of a vocal fold replica with unilateral surface growths, *J. Acoust. Soc.*  
539 *Am.* 141 (2017) 3050–3058.  
540 [13] M. Fatehi Nia, M. H. Akrami, Bifurcation and chaos in a one mass discrete time vocal fold dynamical model, *Int. J.*  
541 *Nonlinear. Anal. Appl.* 12 (2021) 305–315.  
542 [14] J. Cisonni, A. Van Hirtum, X. Pelorson, J. Willems, Theoretical simulation and experimental validation of inverse quasi-  
543 one-dimensional steady and unsteady glottal flow models, *J. Acoust. Soc. Am.* 124 (2008) 535–545.  
544 [15] R. Mittal, B. D. Erath, M. W. Plesniak, Fluid dynamics of human phonation and speech, *Annu. Rev. Fluid Mech.* 45  
545 (2013) 437–467.  
546 [16] G. A. Leonov, N. V. Kuznetsov, Hidden attractors in dynamical systems. from hidden oscillations in hilbert–kolmogorov,  
547 aizerman, and kalman problems to hidden chaotic attractor in chua circuits, *Int. J. Bifurc. Chaos* 23 (2013) 1330002.  
548 [17] Z. Wei, W. Zhang, Z. Wang, M. Yao, Hidden attractors and dynamical behaviors in an extended rikitake system, *Int. J.*  
549 *Bifurc. Chaos* 25 (2015) 1550028.  
550 [18] Z. Wei, W. Zhang, M. Yao, On the periodic orbit bifurcating from one single non-hyperbolic equilibrium in a chaotic jerk  
551 system, *Nonlinear Dyn.* 82 (2015) 1251–1258.  
552 [19] Z. Wei, I. Moroz, J. C. Sprott, Z. Wang, W. Zhang, Detecting hidden chaotic regions and complex dynamics in the  
553 self-exciting homopolar disc dynamo, *Int. J. Bifurc. Chaos* 27 (2017) 1730008.  
554 [20] Z. Wei, W. Zhang, Hidden hyperchaotic attractors in a modified lorenz–steflo system with only one stable equilibrium,  
555 *Int. J. Bifurc. Chaos* 24 (2014) 1450127.  
556 [21] Z. Wei, P. Yu, W. Zhang, M. Yao, Study of hidden attractors, multiple limit cycles from hopf bifurcation and boundedness  
557 of motion in the generalized hyperchaotic rabinovich system, *Nonlinear Dyn.* 82 (2015) 131–141.  
558 [22] Z. Wei, I. Moroz, J. Sprott, A. Akgul, W. Zhang, Hidden hyperchaos and electronic circuit application in a 5d self-exciting  
559 homopolar disc dynamo, *Chaos* 27 (2017) 033101.  
560 [23] M. Broniatowski, S. Kaneko, G. Jacobs, Y. Nose, H. M. Tucker, Laryngeal pacemaker. Part II. Electronic pacing of  
561 reinnervated posterior cricoarytenoid muscles in the canine, *Laryngoscope* 95 (1985) 1194–1198.  
562 [24] M. Broniatowski, H. M. Tucker, S. Kaneko, G. Jacobs, Y. Nose, Laryngeal pacemaker. Part I. Electronic pacing of  
563 reinnervated strap muscles in the dog, *Otolaryngol. Head Neck Surg.* 94 (1986) 41–44.

- 564 [25] D. Goldfarb, W. M. Keane, L. D. Lowry, Laryngeal pacing as a treatment for vocal fold paralysis, *J. Voice* 8 (1994)  
565 179–185.
- 566 [26] D. L. Zealear, C. R. Billante, M. S. Courey, J. L. Netterville, R. C. Paniello, I. Sanders, G. D. Herzon, G. S. Goding,  
567 W. Mann, H. Ejnell, et al., Reanimation of the paralyzed human larynx with an implantable electrical stimulation device,  
568 *Laryngoscope* 113 (2003) 1149–1156.
- 569 [27] A. H. Mueller, R. Hagen, G. Foerster, W. Grossmann, K. Baumbusch, C. Pototschnig, Laryngeal pacing via an implantable  
570 stimulator for the rehabilitation of subjects suffering from bilateral vocal fold paralysis: a prospective first-in-human study,  
571 *Laryngoscope* 126 (2016) 1810–1816.
- 572 [28] A. H. Mueller, Laryngeal pacing, in: *Neurolaryngology*, Springer, 2018, pp. 173–183.
- 573 [29] J. J. Jiang, Y. Zhang, J. Stern, Modeling of chaotic vibrations in symmetric vocal folds, *J. Acoust. Soc. Am.* 110 (2001)  
574 2120–2128.
- 575 [30] E. Ott, C. Grebogi, J. A. Yorke, Controlling chaos, *Phys. Rev. Lett.* 64 (1990) 1196.
- 576 [31] S. L. de Souza, I. L. Caldas, Controlling chaotic orbits in mechanical systems with impacts, *Chaos Solit. Fractals* 19  
577 (2004) 171–178.
- 578 [32] K. Pyragas, Continuous control of chaos by self-controlling feedback, *Phys. Lett. A* 170 (1992) 421–428.
- 579 [33] K. Pyragas, A. Tamaševičius, Experimental control of chaos by delayed self-controlling feedback, *Phys. Lett. A* 180 (1993)  
580 99–102.
- 581 [34] S. Boccaletti, C. Grebogi, Y.-C. Lai, H. Mancini, D. Maza, The control of chaos: theory and applications, *Phys. Reports*  
582 329 (2000) 103–197.
- 583 [35] K. Pyragas, Delayed feedback control of chaos, *Phil. Trans. Roy. Soc. A* 364 (2006) 2309–2334.
- 584 [36] H. Wernecke, B. Sándor, C. Gros, Chaos in time delay systems, an educational review, *Phys. Reports* 824 (2019) 1–40.
- 585 [37] S. De Souza, I. Caldas, R. Viana, J. M. Balthazar, R. Brasil, Impact dampers for controlling chaos in systems with limited  
586 power supply, *J. Sound Vib.* 279 (2005) 955–967.
- 587 [38] J.-Y. Lee, J.-J. Yan, Control of impact oscillator, *Chaos Solit. Fractals* 28 (2006) 136–142.
- 588 [39] S. L. De Souza, I. L. Caldas, R. L. Viana, J. M. Balthazar, Control and chaos for vibro-impact and non-ideal oscillators,  
589 *J. Theor. Appl. Mech.* 46 (2008) 641–664.
- 590 [40] G. Luo, X. Lv, Controlling bifurcation and chaos of a plastic impact oscillator, *Nonlinear Anal. Real World Appl.* 10  
591 (2009) 2047–2061.
- 592 [41] V. Tereshko, R. Chacón, V. Preciado, Controlling chaotic oscillators by altering their energy, *Phys. Lett. A* 320 (2004)  
593 408–416.
- 594 [42] V. Tereshko, Control and identification of chaotic systems by altering their energy, *Chaos Solit. Fractals* 40 (2009)  
595 2430–2446.
- 596 [43] S. L. de Souza, I. L. Caldas, R. L. Viana, Damping control law for a chaotic impact oscillator, *Chaos Solit. Fractals* 32  
597 (2007) 745–750.
- 598 [44] F. A. Hassani, Q. Shi, F. Wen, T. He, A. Haroun, Y. Yang, Y. Feng, C. Lee, Smart materials for smart healthcare—moving  
599 from sensors and actuators to self-sustained nanoenergy nanosystems, *Smart Mat. Med.* (2020).
- 600 [45] M. Arnela, O. Guasch, F. Aliás, Effects of head geometry simplifications on acoustic radiation of vowel sounds based on  
601 time-domain finite-element simulations, *J. Acoust. Soc. Am.* 134(4) (2013) 2946–2954.
- 602 [46] M. Arnela, S. Dabbaghchian, R. Blandin, O. Guasch, O. Engwall, A. Van Hirtum, X. Pelorson, Influence of vocal tract  
603 geometry simplifications on the numerical simulation of vowel sounds, *J. Acoust. Soc. Am.* 140 (2016) 1707–1718.
- 604 [47] O. Guasch, M. Arnela, R. Codina, H. Espinoza, A stabilized finite element method for the mixed wave equation in an  
605 ALE framework with application to diphthong production, *Acta Acust. united Ac.* 102 (2016) 94–106.
- 606 [48] S. Dabbaghchian, M. Arnela, O. Engwall, O. Guasch, Simulation of vowel-vowel utterances using a 3D biomechanical-  
607 acoustic model, *Int. J. Numer. Meth. Biomed. Eng.* 37 (2021) e3407.
- 608 [49] A. M. Fraser, H. L. Swinney, Independent coordinates for strange attractors from mutual information, *Phys. Rev. A* 33  
609 (1986) 1134.
- 610 [50] A. Van Hirtum, A. Bouvet, X. Pelorson, Quantifying the auto-oscillation complexity following water spraying with interest  
611 for phonation, *Phys. Rev. E* 100 (2019) 043111.
- 612 [51] B. Blazéjczyk, T. Kapitaniak, J. Wojewoda, J. Brindley, Controlling Chaos in Mechanical Systems, *Appl. Mech. Rev.* 46  
613 (1993) 385–391.
- 614 [52] M. Lakshmanan, K. Murali, Chaos in nonlinear oscillators: controlling and synchronization, volume 13, World scientific,  
615 1996.
- 616 [53] M. Akhmet, M. Fen, Chaotic period-doubling and ogy kntrol for the forced duffing equation, *Commun. Nonlinear Sci.*  
617 *Numer. Simul.* 17 (2012) 1929–1946.
- 618 [54] S. Ma, Q. Lu, Z. Feng, Double hopf bifurcation for van der pol-duffing oscillator with parametric delay feedback control,  
619 *J. Math. Anal. Appl.* 338 (2008) 993–1007.
- 620 [55] Y. Cao, A nonlinear adaptive approach to controlling chaotic oscillators, *Phys. Lett. A* 270 (2000) 171–176.
- 621 [56] L.-Q. Chen, Y.-Z. Liu, A modified exact linearization control for chaotic oscillators, *Nonlinear Dyn.* 20 (1999) 309–317.
- 622 [57] V. Astakhov, V. Anishchenko, T. Kapitaniak, A. Shabunin, Synchronization of chaotic oscillators by periodic parametric  
623 perturbations, *Phys. D* 109 (1997) 11–16.
- 624 [58] T. Kapitaniak, Controlling chaotic oscillators without feedback, *Chaos Solit. Fractals* 2 (1992) 519–530.
- 625 [59] R. Lin, D. Ewins, Chaotic vibration of mechanical systems with backlash, *Mech. Syst. Signal Pr.* 7 (1993) 257–272.
- 626 [60] J. Sepulchre, A. Babloyantz, Controlling chaos in a network of oscillators, *Phys. Rev. E* 48 (1993) 945.
- 627 [61] L. Xiang, Y. Jia, A. Hu, Bifurcation and chaos analysis for multi-freedom gear-bearing system with time-varying stiffness,  
628 *Appl. Math. Model.* 40 (2016) 10506–10520.

- 629 [62] S. M. Mirvakili, A. Pazukha, W. Sikkema, C. W. Sinclair, G. M. Spinks, R. H. Baughman, J. D. Madden, Niobium  
630 nanowire yarns and their application as artificial muscles, *Adv. Funct. Mater.* 23 (2013) 4311–4316.
- 631 [63] S. M. Mirvakili, I. W. Hunter, Artificial muscles: Mechanisms, applications, and challenges, *Acta Math.* 30 (2018) 1704407.
- 632 [64] Q. Zhang, C. Huang, F. Xia, J. Su, Electric EAP, in *Electroactive Polymer (EAP) Actuators as Artificial Muscles: Reality,*  
633 *Potential, and Challenges*, Y. Bar-Cohen (Ed.), SPIE press, pp. 95–148.
- 634 [65] V. Giovinco, P. Kotak, V. Cichella, C. Maletta, C. Lamuta, Dynamic model for the tensile actuation of thermally and  
635 electro-thermally actuated twisted and coiled artificial muscles (TCAMs), *Smart Mat. Struct.* 29 (2019) 025004.
- 636 [66] Y. Yang, Z. Kan, Y. Zhang, Y. A. Tse, M. Y. Wang, A novel variable stiffness actuator based on pneumatic actuation and  
637 supercoiled polymer artificial muscles, in: 2019 International Conference on Robotics and Automation (ICRA), IEEE, pp.  
638 3983–3989.